# 1 The influence of a rock glacier on the riverbed hydrological system

- 2 Bastien Charonnat<sup>1,6,7</sup>, Michel Baraer<sup>1,6,7</sup>, Eole Valence<sup>2,6</sup>, Janie Masse-Dufresne<sup>1,6,7</sup>, Chloé Monty<sup>3</sup>,
- 3 Kaiyuan Wang<sup>4</sup>, Elise Devoie<sup>5</sup>, Jeffrey M. McKenzie<sup>2</sup>

4 5

6

- <sup>1</sup>Hydrology, Climate and Climate Change laboratory École de technologie supérieure (ÉTS), Montreal, Quebec, Canada
- <sup>2</sup> Department of Earth and Planetary Science McGill University, Montreal, Quebec, Canada
- <sup>3</sup> Department of Earth Sciences Simon Fraser University, Burnaby, British Columbia, Canada
- 8 Department of Earth, Environmental & Planetary Sciences Brown University, Providence, Rhode Island, United States
- 9 <sup>5</sup> Civil Engineering department Queen's University, Kingston, Ontario, Canada
- 10 <sup>6</sup> GEOTOP (Research Centre on the Dynamics of the Earth System), Montreal, Quebec, Canada
  - <sup>7</sup> CentrEau (Ouebec Research Water Centre), Ouebec City, Ouebec, Canada

11 12 13

14

26

Correspondence to: Bastien Charonnat (bastien.charonnat.1@ens.etsmtl.ca)

### Abstract

- 15 Climate change is accelerating cryosphere degradation in mountainous regions, altering hydrological and geomorphological
- dynamics in deglaciating catchments. Among cryospheric features, rock glaciers degrade more slowly than glaciers, providing
- 17 a sustained influence on water resources in alpine watersheds. This study investigates the role of a rock glacier interacting with
- 18 the Shár Shaw Tagà River (Grizzly Creek) riverbed in the St. Elias Mountains (Yukon, Canada), using a unique multimethod
- 19 approach that integrates hydro-physicochemical and isotopic characterization, drone-based thermal infrared (TIR) imagery,
- and visible time-lapse (TL) imagery. Results assess that rock glaciers, due to their geomorphic properties, can constrict
- 21 riverbeds and alluvial aquifers, and control shallow groundwater flow, leading to notable changes in channel structure and
- 22 groundwater discharge. These disruptions promote downstream cryo-hydrological processes by facilitating aufeis formation
- and modifying the physicochemical properties of streamflow. Additional findings highlight the critical role of rock glaciers
- 24 and proglacial systems in connecting mountain cryosphere and deep groundwater systems, with consequent implications for
- 25 mountain hydrology and water resources.

### 1. Introduction

- 27 Climate change is profoundly transforming mountain regions, where the cryosphere plays a critical role in regulating water
- 28 resources essential for the sustainability of downstream ecosystems and communities. With rising global temperatures, high
- 29 mountain areas are experiencing accelerated deglaciation, characterized by glacial retreat and permafrost thaw (Hock et al.,
- 30 2019). These processes drive rapid geomorphological and hydrological reconfigurations in proglacial systems (Carrivick and
- Heckmann, 2017). Understanding the impacts of cryosphere degradation on mountain hydrology and hydrogeology is essential

33 has been identified as a critical issue in mountain hydrology, directly influencing water resource sustainability under changing 34 climatic conditions (van Tiel et al., 2024). 35 In proglacial systems, riverbeds and outwash plains serve as critical hydrogeological components, sustaining baseflow and 36 aquatic habitats (Käser and Hunkeler, 2016; Müller et al., 2024). However, the recharge and discharge dynamics of alluvial 37 groundwater systems are intrinsically linked to upstream and adjacent cryospheric features (e.g., glaciers, seasonal snowpacks, 38 etc.; Müller et al., 2024), as evidenced by aufeis formation. Aufeis, or icings, are layered ice formations that develop in winter 39 when groundwater outflows persist under sub-zero temperatures for several months (Ensom et al., 2020). These formations 40 can occur due to upwellings of groundwater encountering impermeable permafrost (Terry et al., 2020), with channel 41 constriction further promoting their formation (Wainstein et al., 2014; Liu et al., 2021). In mountain environments, aufeis 42 formations are common in outwash plains and are generally supplied by groundwater and meltwater from surrounding 43 cryospheric sources (Chesnokova et al., 2020; Mallinson et al., 2019; Wainstein et al., 2014). 44 Among cryospheric features, rock glaciers degrade more slowly than glaciers, allowing them to exert a prolonged influence 45 on hydrological processes as glaciers retreat (Bolch and Marchenko, 2009; Harrison et al., 2021; Jones et al., 2021). Despite 46 growing recognition of their hydrological importance, rock glaciers remain understudied compared to glaciers, particularly 47 concerning their roles in deglaciating catchments (Jones et al., 2019). Rock glaciers are tongue-shaped landforms composed 48 of rocky debris and ice, which creep due to the deformation of the ice-debris matrix, concentrated in the shear horizon (Arenson 49 et al., 2002). They are commonly found in high mountain environments and occur in both discontinuous and continuous 50 permafrost zones (Barsch, 1996). While existing studies primarily focus on the internal hydrological behavior of rock glaciers, 51 research addressing their broader catchment-scale implications remains limited (Jones et al., 2019). 52 Rock glaciers have been shown to buffer surface waters throughout the year, sustaining baseflow during dry periods and 53 attenuating discharge response to intense precipitation events due to their internal structure (Bearzot et al., 2023; Reato et al., 54 2022; Wagner et al., 2021). Their hydrological behaviour is closely tied to the distribution of frozen and liquid water within 55 them (Harrington et al., 2018; Wagner et al., 2016; Winkler et al., 2016). Unfrozen layers in summer can act as reservoirs and 56 conduits for water flow (Halla et al., 2021; Harrington et al., 2018; Navarro et al., 2023; Wagner et al., 2020). In addition to 57 liquid water, intact rock glaciers (i.e., containing frozen content) store significant volumes of solid water as interstitial or 58 massive ice (Chakravarthi et al., 2022; Halla et al., 2021; Jones et al., 2018; Wagner et al., 2021). However, internal ice melt 59 typically contributes only minimally to total rock glacier discharge (Arenson et al., 2022). In addition to modulating discharge, 60 rock glaciers influence downstream water quality by increasing solute concentrations (Colombo et al., 2018; Colombo et al., 61 2019; Schreder et al., 2023; Engel et al., 2019; Wanner et al., 2023; Zarroca et al., 2021) and cooling stream temperatures 62 (Bearzot et al., 2023; Brighenti et al., 2019; Colombo et al., 2020). The physicochemical impact of rock glacier outflows is 63 particularly pronounced at the catchment scale when compared to catchments lacking glacial or periglacial landforms

for predicting future water availability in these regions. Recently, the connectivity between the cryosphere and groundwater

32

64

(Brighenti et al., 2023; Clow et al., 2021; Del Siro et al., 2023; Gammons et al., 2021; Robinson et al., 2022).

While much of the literature focuses on the downstream effects of rock glacier outflows (e.g., Brighenti et al., 2023; Robinson et al., 2022; Wagner et al., 2016; Wagner et al., 2021), their influence on the hydrogeomorphology of riverbeds and outwash plains remains understudied. Rock glaciers can advance, constrain, and dam riverbeds, potentially forming ponds, as reported in High Asia (Blöthe et al., 2019; Falatkova et al., 2020; Hewitt, 2014) and the Alps (Colombo et al., 2020). Furthermore, topographic changes driven by glacial retreat and paraglacial processes can force channel confinement (Marren and Toomath, 2014). Climate change has intensified rock glacier movement (Delaloye et al., 2010; Kummert et al., 2019; PERMOS, 2019), sometimes causing destabilization (Marcer et al., 2021) and channel disruption (Sorg et al., 2015). Additionally, sudden mass movements, such as the catastrophic collapse of rock glacier lobes, have triggered debris flows with downstream geomorphic impacts (Bodin et al., 2015; Scotti et al., 2017). The hydrological and geomorphic disturbances caused by advancing rock glaciers in valley systems are particularly notable, given the critical role of riverbeds and outwash plains in sustaining water resources. Despite recent studies (e.g., Falatkova et al., 2020; Wagner et al., 2021), research on the interactions between rock glaciers, the adjacent cryosphere, surface waters, and groundwater flow within valley systems is still underexplored.

This study examines the influence of rock glaciers on surface and shallow groundwater flow within alpine riverbed hydrological systems. Specifically, it focuses on characterizing water fluxes in a section of the Shár Shaw Tagà catchment (St. Elias Mountains, Yukon, Canada) that is constrained by a rock glacier. We hypothesize that the rock glacier modulates interactions between surface water and shallow groundwater, thereby affecting the overall functioning of the riverbed system. To investigate these interactions, we employed a multimethod approach that was progressively refined as our observations and understanding of the system evolved:

- 1) We hypothesized that the rock glacier influences the formation of aufeis on the downstream outwash plain. To test this, we used time-lapse camera monitoring to track the development of aufeis and to identify the location and timing of winter outflows.
- 2) Given the rock glacier's position at the outlet of a subcatchment and the lack of significant surface outflow, we hypothesized that it drains the subcatchment and contributes to river discharge via groundwater exfiltration. To assess this, we conducted a spring inventory, followed by a physico-hydrochemical characterization of springs and streams across the subcatchment. This allowed us to trace water sources and evaluate the rock glacier's influence on stream composition.
- 3) Building on the previous findings, we hypothesized that a specific section of the riverbed serves as a major zone of groundwater exfiltration. To identify and map these zones, we conducted drone-based thermal infrared (TIR) surveys, enabling us to delineate areas of groundwater emergence and assess their spatial extent and relative magnitude.

The novelty of this research lies in its focus on the indirect hydrological impacts of a rock glacier—particularly in the absence of a visible, well-defined outflow. By integrating hydrological, hydrogeological, and geochemical methods, this study advances our understanding of the complex role rock glaciers play in alpine watershed dynamics, and provides insights with broader applicability to similar environments worldwide.

# 2. Study site

98

99

100

101

102

103104

105

106

107

108

109

110

111

112

113

114

115

Shár Shaw Tagà, meaning Grizzly Creek in the Southern Tutchone indigenous language, is a 32 km<sup>2</sup> glacierized catchment located within the traditional lands of the Kluane First Nation and the White River First Nation (Fig. 1a). It also lies within the boundaries of Kluane National Park and Reserve in the St. Elias Mountains, southwestern Yukon Territory, Canada (61°05'13" N, 139°07'18" W). The eastern flank of the St. Elias Mountains experiences a dry subarctic climate, characterized by annual precipitation ranging from 300 to 500 mm yr<sup>-1</sup> and a mean annual temperature between -8 °C and -12 °C (Wahl et al., 1987). The upper Shár Shaw Tagà catchment (Fig. 1b) contains eight glaciers, the largest of which is G-A1, covering an area of 3.2 km<sup>2</sup>. Faults are inferred along the valley floor (Dodds and Campbell, 1992). Due to its heavily fractured bedrock lithology and steep slopes, the valley is characterized by significant mass wasting processes and depositional features, including nine previously identified rock glaciers (Johnson, 1978; Evin et al., 1997). Between 1974 and 1997, Johnson participated to a series of geomorphological studies on the valley (Johnson, 1974; 1978; 1980; 1983; 1986; 1992; Evin et al., 1997), providing detailed descriptions of its landforms. The geomorphological identification and landform naming for these features, as established in Johnson's works, are adopted in this study to characterize the geomorphological setting. The significance of ground ice landforms in the valley has prompted recent investigations, including a study on buried ice detection using ground-penetrating radar (GPR) in rocky and steep terrains (Tjoelker et al., 2024). Publications prior to 2024 referred to the area by the toponym "Grizzly Creek" rather than Shár Shaw Tagà. Of the nine rock glaciers identified by Johnson and Evin et al. (1978; 1997), seven extend into the riverbed along the valley floor, with some exerting considerable geomorphological constraints on the stream.

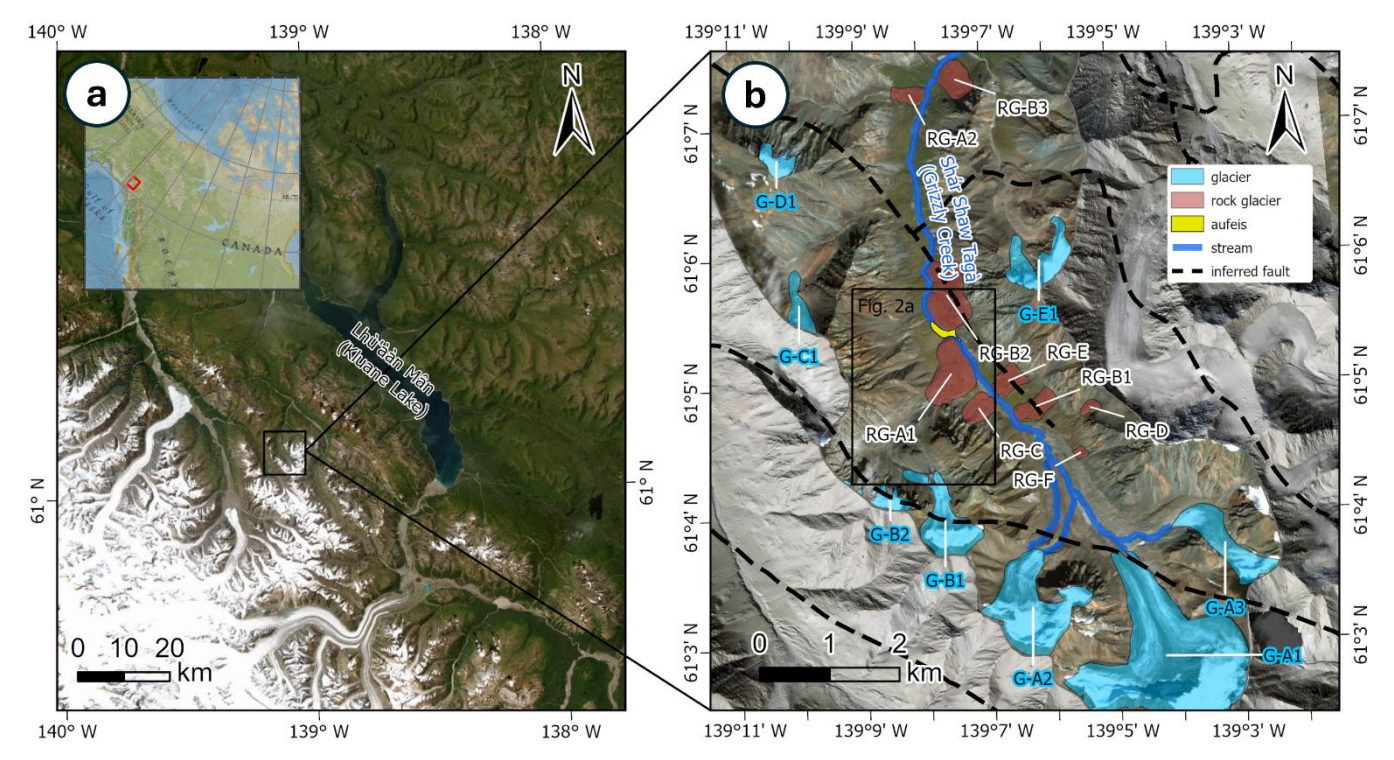


Fig. 1: (a) Overview map showing the location of the Shár Shaw Tagà valley in southwestern Yukon, Canada. (b) Enlarged view of the study area from panel (a), highlighting key geomorphological features. The black frame outlines the extent of the map shown in Fig. 2a. ArcticDEM data: Polar Geospatial Center (Porter et al., 2023). Basemap credits: Esri.

The present study investigates the hydrological influence of the RG-A1 rock glacier, located on the western side of the upper Shár Shaw Tagà valley. RG-A1, first identified by Johnson (1978), spans elevations between 1700 and 1850 m a.s.l. The southern lobes of RG-A1 appear older, characterized by vegetation cover and a smoother frontal morphology, while the northern lobes are younger, with sparse or absent vegetation, sharper forms, and a steeper front (Johnson, 1978). A frozen layer, 20 to 40 m thick was detected in RG-A1 during a previous geophysical study, which also suggested the presence of massive ice lenses at depth (Evin et al., 1997). The front of RG-A1 advances in the valley, constraining the Shár Shaw Tagà River against the opposing talus slope. Although previous studies did not classify the opposing talus slope as a rock glacier, it is suspected to be a protalus rampart (or small active rock glacier) based on environmental and topographic criteria outlined in Scapozza (2015), such as the absence of an upstream permanent snow field, the presence of coarse boulders in the upslope area, a steep front with exposed fine sediments, and its juxtaposition and superimposition to other rock glaciers.

The outwash plains upstream and downstream of RG-A1 are separated by a "narrow section" of the Shár Shaw Tagà River.

The outwash plains upstream and downstream of RG-A1 are separated by a "narrow section" of the Shár Shaw Tagà River, which can be divided into two subsections: N1 and N2 (Fig. 2). N1 extends from the outlet of the upstream outwash plain to a bedrock outcrop visible on the opposite talus slope to RG-A1. N2 extends from this bedrock outcrop to the outlet of the "narrow section", where the rivers enters the downstream outwash plain. An aufeis forms in winter in the downstream outwash plain,

- as confirmed through field studies since 2018 and satellite imagery. No aufeis has been detected in the upstream outwash plain
- during this period.
- 137 In 1974, Johnson (1978) observed that meltwater drained into a sinkhole located in the rooting zone of RG-A1 (at
- approximately 1850 m a.s.l.), with no major resurgence observed at the front (at 1700 m a.s.l.). In 1975, a new sinkhole was
- observed upstream of the first one, and a significant resurgence was reported on the northern part of RG-A1. Dry channels on
- the surface of RG-A1 in 1975 were interpreted by Johnson as abandoned surface drainage pathways, highlighting the dynamic
- and variable hydrological behaviour of RG-A1.
- Field observations by our research team from 2018 to 2023 confirm the absence of a significant visible outlet from the rock
- glacier, despite its location downstream of a 8 km<sup>2</sup> subcatchment, consisting of the G-B1 and G-B2 glaciers. The only visible
- outlets consist of low-discharge springs around the RG-A1 front, particularly concentrated along the N1 subsection. During
- low-discharge periods such as June 2023, we observed that the water from the Shár Shaw Tagà River infiltrates the riverbed,
- leaving it dry before entering the outwash plain upstream of RG-A1. However, water was observed to flow again within the
- riverbed in the N1 subsection, visually sustained by springs and seepage. During high-flow periods, the springs emerge directly
- under the front of RG-A1. In dry periods, like June 2023, the springs shift away from the front and align with the current river
- level, 10 to 20 m downstream.

### 3. Methods

150

159

160

# 151 **3.1 TL monitoring**

- Two RGB timelapse (TL) cameras, designated TL1 and TL2, were positioned above the right bank of the Shár Shaw Tagà
- River (61°5'26" N, 139°7'34" W; Fig. 2). TL1 was installed in 2018, focused on the central area of the outwash plain
- immediately downstream of RG-A1. In 2019, TL2 was added adjacent to TL1, extending its field of view from the upper
- margin of TL1's coverage to the outlet of the N2 subsection of the Shár Shaw Tagà River. Both cameras were configured to
- capture four images daily at 8:00, 11:00, 13:00, and 16:00. The visual analysis of the images captured by the TL cameras
- 157 involved identifying signs of surface overflow on the developing aufeis and documenting the occurrence of such events
- throughout the winter, following the protocol outlined by Chesnokova et al. (2020).

### 3.2 Physico-hydrochemical characterisation

#### 3.2.1 Sampling and field measurements

- 161 Physico-hydrochemical characterisation was undertaken over three distinct campaigns: June 2022, August 2022, and June
- 162 2023. These campaigns targeted both the Shár Shaw Tagà River and springs inventoried from 2018 to 2021, capturing different
- hydrological conditions. The June 2022 campaign coincided with the melt of a late and substantial snowpack. The August
- 164 2022 campaign took place during late summer, when glacial ablation was at its peak. The June 2023 campaign was conducted

- following a winter with reduced snowpack and early snowmelt, after the primary snowmelt phase but before summer glacial
- ablation commenced, while glaciers remained snow-covered.
- 167 Field measurements included in situ pH, electrical conductivity (EC, corrected to 25 °C, expressed in µS cm<sup>-1</sup>), and water
- temperature (°C). Water samples were collected for laboratory analyses. Additionally, in June 2023, in situ radon
- 169 measurements were performed to further investigate groundwater contributions. Measurements were taken at each sampling
- site using a calibrated Hanna HI 98195 multiparameter meter.
- Water sampling followed a synoptic approach for cycles of 1-2 days, avoiding precipitation periods (e.g. Baraer et al., 2009).
- When possible, sites were sampled multiple times within each campaign to account for diurnal fluctuations in physicochemical
- parameters. Samples were categorized into four types (Table A1): glacial outlets from the RG-B1 snout (S-GL#), streams in
- the ice-debris complex located between the RG-B1 snout and RG-A1 (S-IDC#), springs at the RG-A1 front and opposite talus
- 175 (S-RG#), and Shár Shaw Tagà River (S-R#). Water samples were filtered using 0.45 µm syringe filters and collected in 50 mL
- HDPE bottles, rinsed three times prior to sampling. Not all sites were accessible during each campaign (Table A1), due to
- factors such as no flow or safety concerns related to snow cover and rockfalls.
- Results were analyzed following the methodology of Baraer et al. (2015). Samples for major ion analysis were stored in a dark
- environment at 4 °C until analysis. Major ions (Ca<sup>2+</sup>, Mg<sup>2+</sup>, Na<sup>+</sup>, Cl<sup>-</sup>, SO<sub>4</sub><sup>2-</sup>) and minor ions (K<sup>+</sup>, F<sup>-</sup>) were analyzed at the LG2
- laboratory, École de technologie supérieure (ÉTS), Montreal, Canada, Cation concentrations were determined using an
- inductively coupled plasma optical emission spectrometer (5110 ICP-OES, Agilent), and anion concentrations were measured
- with an ion chromatograph (Dionex ED50, Thermo Fisher Scientific), Bicarbonate (HCO<sub>3</sub><sup>-</sup>) concentrations were calculated
- from the charge balance equation, and total dissolved solids (TDS) were derived from the sum of ion concentrations.
- Stable isotopic composition of the water molecule ( $\delta^{18}O$  and  $\delta^{2}H$ ) was measured using a cavity ringdown spectrometer (Picarro
- 185 L2130-i) at the LG2 laboratory (ÉTS), Montreal, Canada, expressed in % relative to Vienna Standard Mean Ocean Water
- (VSMOW). Internal reference waters were used for normalization after every 3 injections. The analytical uncertainty is  $\pm 0.13$
- 187 % for  $\delta^{18}$ O and  $\pm 1.5$  % for  $\delta^{2}$ H. The nearest local meteoric water line (LMWL) is established for the Whitehorse area 220 km
- 188 east of Shár Shaw Tagà (Birks et al., 2004). The LMWL is similar to isotopic compositions found in the Lhù'ààn Mân' (Kluane
- 189 Lake), 25 km east of Shár Shaw Tagà (Brahney et al., 2010). The LMWL is displayed alongside the analyses results as
- reference (Fig. 6d, Fig. 7d and Fig. 8d) but we prefer not to assume direct applicability to our data...
- 191 Radon (222Rn) serves as a natural tracer to detect groundwater exfiltration in streams (Cartwright and Hofmann, 2016). In situ
- 192 radon activities were measured at four locations in the N1 subsection, including S-RG8 and S-RG9A springs, and at the
- upstream and downstream ends of the N1 subsection (S-RUP and S-R1, respectively). A portable RAD7 Radon Monitor
- 194 (Durridge) was used, coupled with the Rad Aqua accessory (Durridge) for radon degassing. Results are reported in Bq m<sup>-3</sup>,
- with an analytical uncertainty of  $\pm$  220 Bg m<sup>-3</sup>.

### 3.2.2 Principal Component Analysis and clustering

- 198 Principal Component Analysis (PCA) was employed to classify the origins of the sampled water and to identify sample groups
- that influence the chemistry of the Shár Shaw Tagà River. For each of the three sampling campaigns, PCA was performed
- using a set of independent variables: water temperature,  $\delta^{18}O$ , Na<sup>+</sup>, Mg<sup>2+</sup>, Ca<sup>2+</sup>, and SO<sub>4</sub><sup>2-</sup>. These major ions were selected as
- they exhibited concentrations above the detection limit in more than 95 % of the samples. Principal components explaining at
- 202 least 90 % of the total variance were retained for further analysis to ensure the robustness of the PCA.
- After conducting PCA, clustering analysis was performed using the k-means algorithm for each campaign (Lloyd, 1982;
- 204 MacQueen, 1967). This analysis was based on the sample scores derived from the selected principal components. The
- 205 maximum number of clusters was set at 25 % of the total number of samples for each campaign, which corresponded to 5, 9
- and 7 for the campaigns of June 2022, August 2022, and June 2023, respectively. The algorithm determined the resulting
- 207 clusters were by associating samples with dominant combinations of variables, thereby highlighting inherent patterns within
- the dataset.

209

197

### 3.3 TIR survey

- Aerial and handheld thermal infrared (TIR) devices have been demonstrated as effective tools for mapping groundwater
- discharge into streams (Toran, 2019). Specifically, drone-based TIR technology allows for high spatial resolution observations
- of surface water-groundwater interactions (Vélez-Nicolás et al., 2021). Two common approaches for TIR surveys were
- considered: 1) generating stream temperature maps using high-definition TIR image orthomosaics from overlapping images
- 214 (e.g., Abolt et al., 2018; Casas-Mulet et al., 2020; Rautio et al., 2015), and 2) using TIR videos or real-time scans (handheld
- or drone-based) to visualize mixing plumes and record GPS coordinates of observed points (e.g., Barclay et al., 2022; Briggs
- 216 et al., 2016; Iwasaki et al., 2023).
- While georeferenced thermal maps provide mesoscale coverage, they require stable flying conditions, ground control points,
- and extensive post-processing (Webb et al., 2008). In contrast, TIR video or live scans allow for real-time visualization of
- 219 mixing dynamics in smaller-scale areas (Antonelli et al., 2017). Given our goal to identify and characterize groundwater
- 220 exfiltration zones, we chose the TIR video approach. This method does not require precise absolute temperature but relies
- 221 instead on relative contrasts between stream water and suspected groundwater inflows. Prior studies (Antonelli et al., 2017;
- Briggs et al., 2016; Iwasaki et al., 2023; Iwasaki et al., 2024) have shown that TIR video, even without embedded temperature
- scales, effectively highlights such contrasts.
- Drone-based TIR video surveys were conducted on 28 June 2024, between 08:00 and 10:00, to maximize the coverage of
- shaded sections of the stream. The surveys were conducted using a DJI Mavic 3T Enterprise, equipped with a DJI RTK module
- and a DJI D-RTK 2 mobile station for GNSS base-station support. The Mavic 3T features a 48-megapixel RGB camera with
- 227 a 24 mm focal length and a 640 × 512-pixel thermal camera with a 40 mm focal length. The drone was manually controlled to
- optimize the capture of surface temperatures across wide sections of the Shár Shaw Tagà River, recording both TIR and RGB

videos simultaneously. Flight altitudes ranged from 5 to 20 m above ground level, depending on the section. All flights were manually piloted at low altitudes and near-nadir angles to reduce geometric distortion and minimize emissivity-related error (Torgersen et al., 2001; Dugdale et al., 2016). The survey began approximately 180 m upstream of the N1 subsection and ended around 800 m downstream of the N2 subsection (Fig. 2). Due to difficulties in flying over the narrow section, it was surveyed twice at different elevations. The TIR video was visually analyzed to identify cold groundwater exfiltration areas using two criteria: 1) a clear contrast between the dominant stream surface temperature and the suspected exfiltration area, with an area larger than 10 cm<sup>2</sup>, and 2) the presence of a turbulent mixing zone at least 1 m in length immediately downstream of the suspected area (flight data and information are available as Supplemental Material in Charonnat and Baraer, 2025). Absolute temperatures were not derived due to the absence of a calibrated color scale in the TIR video; instead, detection relied on qualitative identification of relative temperature differences appearing as visual color contrasts in the TIR video—typically, colder areas appeared as blue-toned patches compared to the green-toned stream and red-toned sunlit boulders. When both criteria were met, the RGB video was used for confirmation. The Shar Shaw Taga River, originating from glacial melt, has a substantial suspended sediment load, whereas groundwater is nearly free of suspended sediments. This contrast is visible in the RGB video frames. The observed thermal contrasts were consistent with previously measured field temperature differences between springs and stream water, typically >2°C and <6°C (Table S1), and exceeded the uncertainty range of uncorrected thermal imagery under field conditions (Zappa and Jessup, 1998). Finally, images of confirmed groundwater exfiltration areas were extracted from the videos for size evaluation. Exfiltration areas from the left bank were labeled TIR-

229

230

231

232

233

234

235

236

237

238

239

240

241

242

243

244

245

246

247

L#, and those from the right bank were labeled TIR-R#.

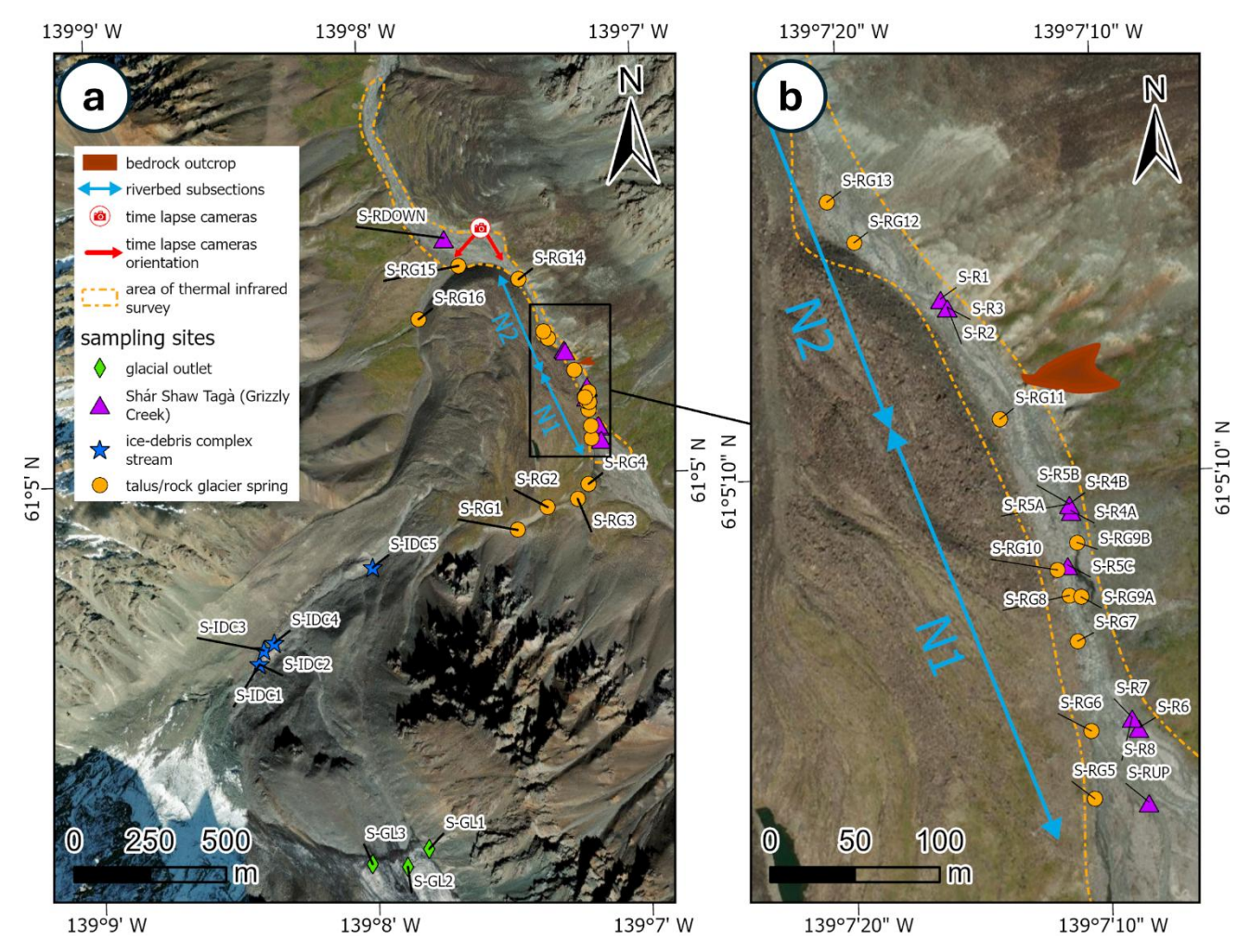


Fig. 2: Map illustrating the methods used in this study. Panel (a) corresponds to the area shown in Fig. 1b, while panel (b) provides a zoom-in of panel (a). A bedrock outcrop on the talus slope opposite to RG-A1 marks the division of the Shár Shaw Tagà River's "narrow section" into two subsections, N1 and N2, as shown on the map. The spring locations represent the outflow points observed during the August 2022 campaign, though their positions may vary depending on hydro-meteorological conditions. Basemap credits: Esri.

### 4. Results

# 4.1 TL monitoring

Between 2018 and 2021, TL1 monitored aufeis formation during the winters of 2018-2019 and 2019-2020 (Fig. 3 and 4a). No aufeis formation was observed during the winter of 2020-2021. The onset of aufeis development varied between the two winters: in 2018-2019, it began in early November and continued to develop throughout the winter season, whereas in 2019-2020, it started in February and progressed through February and March (Fig. 3). The development of the aufeis in both winters

occurred in phases characterized by multiple flood events. Visible ablation of the aufeis began in May, with complete melt occurring by June in both 2019 and 2020. The aufeis that formed during the winters of 2018-2019 and 2019-2020 spanned the entire width of the river, from the RG-A1 front to the RG-B2 front.

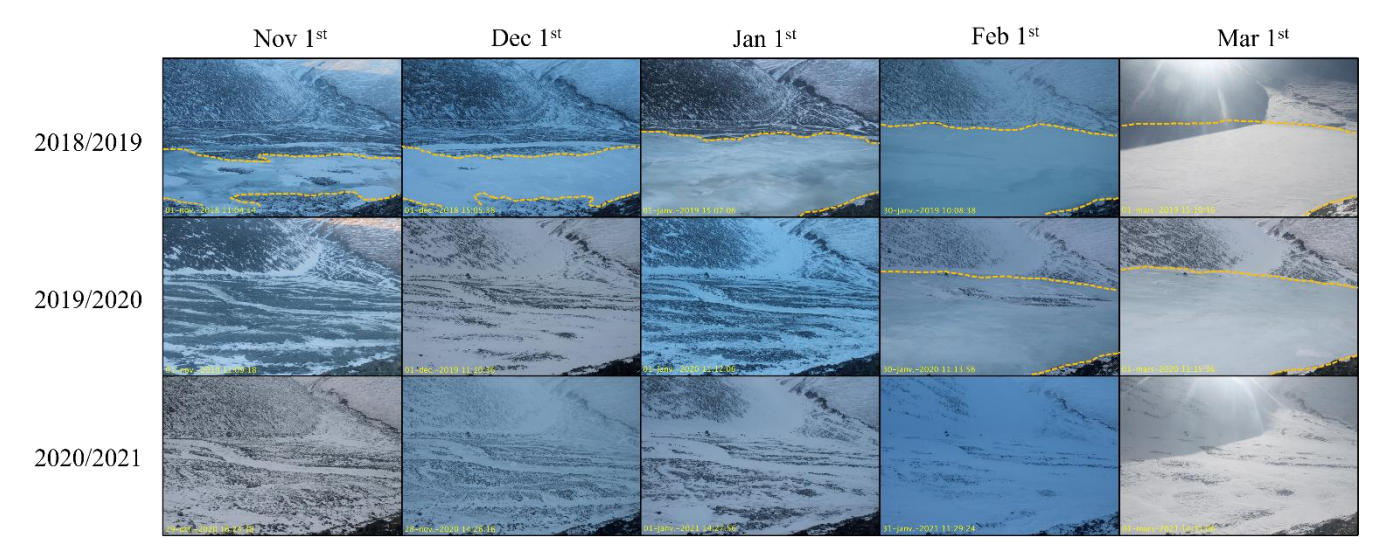
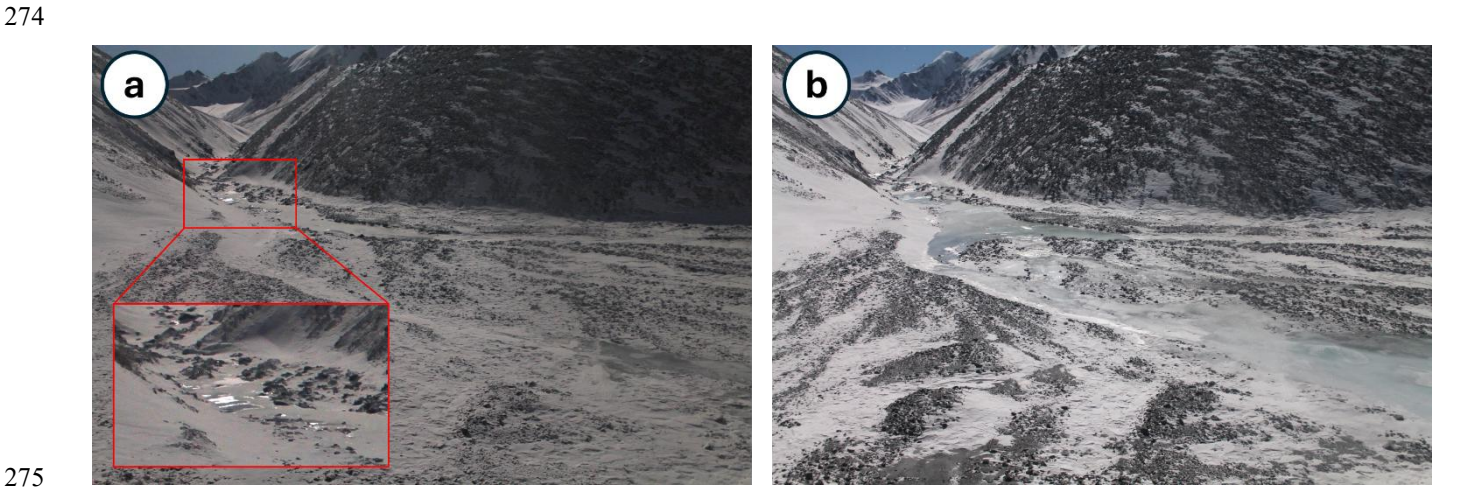


Fig. 3: Monthly timelapse images captured by TL1 of the aufeis from November 1st to March 1st during the winters of 2018-2019, 2019-2020, and 2020-2021. The yellow dashed line indicates the extent of the aufeis in each image when visible. The timelapse images were selected based on the closest date to the first day of each month, with consideration given to image quality. Note that no aufeis formation occurred during the 2020-2021 winter.

TL2, installed in 2019 next to TL1 and oriented upstream, recorded the formation of the aufeis in the winter of 2019-2020 and its absence during 2020-2021. In the winter of 2020, TL2 captured reflections of liquid water and/or ice at the end of the N2 subsection, when the river was dry (Fig. 4). In subsequent days, the aufeis was observed to form in the downstream outwash plain, starting from the end of the N2 subsection. This observation suggests that the overflowing water contributing to the formation of the aufeis originates from the "narrow section" of the Shár Shaw Tagà River.



261

262

263

264 265

266

267

268

269

270

271

272

- Fig. 4: Initiation of an aufeis in the downstream outwash plain, captured by TL2 on (a) 04/01/2020 at 08:00, and (b) 08/01/2020 at
- 277 11:00. The light in the raw images has been enhanced to improve picture quality. Both images are oriented towards the end of the
- N2 subsection and the entrance of the downstream outwash plain. (a) At 8:00 on 04/01/2020, the aufeis has not vet formed, but
- reflections of ice and/or liquid water are visible at the end of the N2 subsection, during a time when the Shár Shaw Tagà River is dry. (b) At 11:00 on 08/01/2020, the aufeis has started to form in the outwash plain, extending from the end of the N2 subsection.
- The repetitive monitoring of the aufeis provides evidence of overflow events during late fall and winter, particularly in the
- 282 2018-2019 and 2019-2020 periods. The formation of the aufeis is attributed to groundwater outflow from the "narrow section"
- of the Shár Shaw Tagà River, as the river runs dry in winter in the downstream outwash plain and no aufeis forms in the
- upstream outwash plain. This finding aligns with the high density of springs inventoried along the N1 subsection.

# 4.2 Physico-hydrochemical characterization

# 4.2.1 Sampling and field measurements

- A high concentration of springs was reported along the N1 subsection of the Shár Shaw Tagà River (S-RG5 to S-RG11) from
- 289 2018 to 2021, and during the 2022 sampling campaigns. This led to a dedicated sampling campaign in June 2023. Many of
- these springs were sampled across multiple campaigns, indicating their long-term flow. The June 2022 and August 2022
- sampling campaigns can be directly compared for the springs at RG-A1's front, given their similar spatial coverage and
- sampling sites. In contrast, the June 2023 sampling campaign focused specifically on the N1 subsection of the river (Table
- 293 A1).

285286

- The mean water temperature for samples collected from the springs at RG-A1's front in June 2022 was 0.90 °C, with a range
- of 3.16 °C, slightly colder than in samples from August 2022, exhibiting a mean temperature of 1.38 °C and a range of 3.77
- <sup>o</sup>C (Table S1). While cold temperatures in June 2022 may have been strongly influenced by recent snowmelt, no snow
- 297 remained at the lower elevations of the catchment in August 2022. In late season, cold groundwater outflows (< 2 °C) suggest
- the possible presence of frozen content in the vicinity of springs (Carturan et al., 2016; Frauenfelder et al., 1998; Haeberli,
- 299 1975; Scapozza, 2009).
- The June 2022 campaign recorded a lower mean EC in springs at RG-A1's front of 225.64 μS cm<sup>-1</sup>, with a range of 439.10 μS
- 301 cm<sup>-1</sup>, compared to 490.82 μS cm<sup>-1</sup> with a range of 546.72 μS cm<sup>-1</sup> in August 2022. These results indicate dilution due to
- 302 snowmelt in early season and increased groundwater contribution in late season, consistent with results from other rock glacier
- 303 hydrology studies (Jones et al., 2019). The high EC ranges highlight the heterogeneous behavior of the sampled springs. Mean
- pH values were 8.47 in June 2022 and 8.13 in August 2022, with ranges of 1.84 and 1.00, respectively.
- The mean isotopic composition was more depleted in the springs at RG-A1's front in June 2022 (-23.57 ‰ vs. VSMOW for
- $\delta^{18}$ O and -183.69 ‰ vs. VSMOW for  $\delta^{2}$ H, with ranges of 1.64 ‰ and 8.78 ‰, respectively) compared to August 2022 (-21.01
- 307 % vs. VSMOW for  $\delta^{18}$ O and -169.20 % vs. VSMOW for  $\delta^{2}$ H, with ranges of 1.38 % and 9.68 %, respectively). This depletion
- is associated with a higher snowmelt contribution in June 2022. Solute concentrations were generally lower in June 2022,
- frequently falling below detection limits for chlorides (all samples < 0.13 mg L<sup>-1</sup>), potassium (13 out of 20 samples < 0.01 mg

 $L^{-1}$ ), sodium (13 out of 20 samples < 0.09 mg  $L^{-1}$ ), and magnesium (1 out of 20 samples < 0.03 mg  $L^{-1}$ ). In contrast, in August 2022, solute concentrations exceeded detection limits for 38 out of 39 samples for all elements except chlorides (36 out of 39 samples < 0.13 mg  $L^{-1}$ ).

The June 2023 campaign showed a mean water temperature for the rock glacier springs of 1.40°C, with a range of 0.23 °C. The mean EC value for June 2023 was 678.43  $\mu$ S cm<sup>-1</sup>, with a range of 172.00  $\mu$ S cm<sup>-1</sup>. The mean pH value was 7.82 with a range of 0.23. The mean isotopic composition for the springs during this campaign was -22.86 % vs. VSMOW for  $\delta^{18}$ O and -178.11 % vs. VSMOW for  $\delta^{2}$ H, with ranges of 0.30 % and 1.10 %, respectively.

In June 2023, while the Shár Shaw Tagà River level was lower than in previous years for the same period,  $^{222}$ Rn activities were similar at S-RG8 and S-RG9A, ranging from  $10.17\times10^3\pm0.22\times10^3$  Bq m<sup>-3</sup> to  $10.85\times10^3\pm0.19\times10^3$  Bq m<sup>-3</sup> (Fig. 5). These springs are located along the N1 subsection of the river, at the left and the right of the stream, respectively. In contrast, the Shár Shaw Tagà River at the upstream end of the N1 subsection (S-RUP) exhibited low activities  $(0.36\times10^3\pm0.06\times10^3$  Bq m<sup>-3</sup>), while the downstream end of N1 (S-R1) showed significantly higher activities  $(5.46\times10^3\pm0.14\times10^3$  Bq m<sup>-3</sup>). These results indicate a major groundwater input to the Shár Shaw Tagà River in the N1 subsection, where S-RG8 and S-RG9A are located.

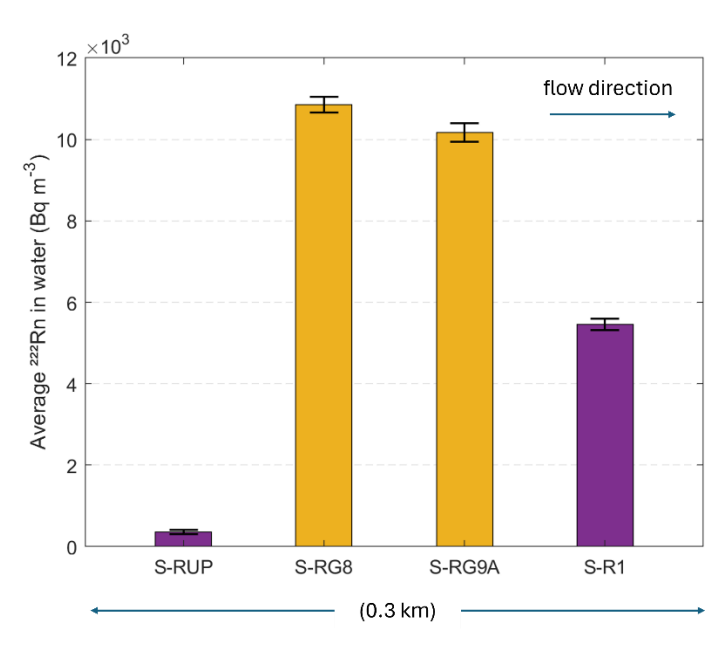


Fig. 5: <sup>222</sup>Rn activities measured with a portable RAD7 Radon Monitor (Durridge) in June 2023. Data were collected at springs S-RG8 and S-RG9A (orange) and along the Shár Shaw Tagà river at upstream (S-RUP) and downstream (S-R1) sites (purple). The bars are arranged from left to right in spatial sequence from upstream to downstream. The error bars represent the uncertainties in the radon activity measurements.

# 4.2.2 Principal Component Analysis and clustering

# Samples collected in June 2022

Principal Component (PC) 1 accounts for 60.96 % of the variance in the dataset and primarily reflects the influence of mineral elements, with PC scores ranging from 0.47 to 0.50 (Fig. 6a). PC2 and PC3, explaining 18.29 % and 14.10 % of the variance, respectively, exhibit contrasting associations with the  $\delta^{18}$ O ratio and temperature. PC2 displays a strong positive correlation with the  $\delta^{18}$ O ratio (0.73) and a negative correlation with temperature (-0.67), whereas PC3 shows positive correlations with  $\delta^{18}$ O (0.62) and temperature (0.71).

Clustering analysis based on PCA reveals two distinct clusters among the June 2022 samples (Fig. 6b). Cluster 1 comprises 17 samples characterized by low concentrations of mineral elements (Fig. 6c), with total dissolved solids (TDS) concentrations ranging from 28 to 100 mg L<sup>-1</sup>. In contrast, Cluster 2 includes samples S-RG4, S-RG5, and S-RG8, which show elevated TDS values (90 to 269 mg L<sup>-1</sup>). With the exception of S-RUP, S-RG4, and S-RG15, which record warmer temperatures from 1.43 to 3.19 °C, the remaining 16 samples in the June 2022 dataset exhibit colder temperatures, ranging from 0.03 °C to 0.67 °C (Fig. 6c). The most enriched samples are S-RG7, S-RG8, and S-RG10, with  $\delta^{18}$ O values between -23 % and -22.6 % vs. VSMOW in  $\delta^{18}$ O (Fig. 6d).

In June 2022, most of the springs were supplied by recent snowmelt, as indicated by low concentrations of mineral elements and cold temperatures. In contrast, S-RG8 and S-RG4 were supplied by groundwater, as evidenced by their higher concentrations of mineral elements.

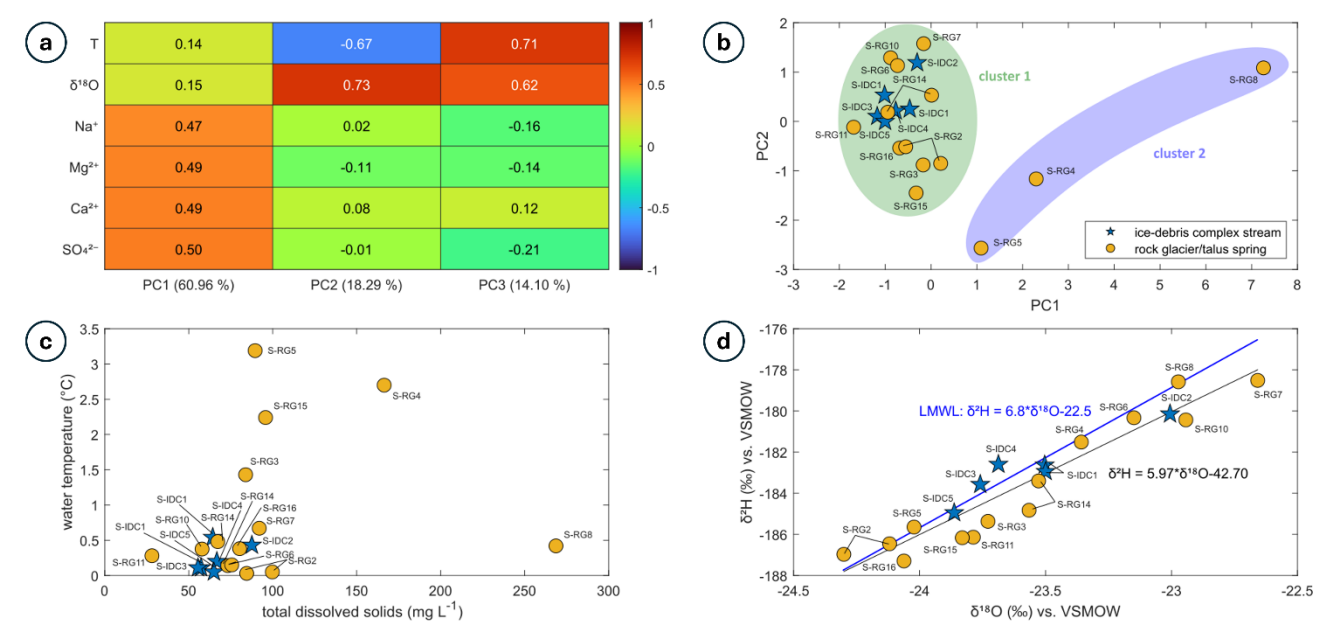


Fig. 6: (a) PCA scores for June 2022 samples. The explained variance for each PC is indicated in the legend of the horizontal axis. (b) Distribution of clusters formed from June 2022 samples following PCA and k-means clustering. Symbols represent different

sample types, and ellipses illustrate the distribution of each cluster. (c) Distribution of total dissolved solids (TDS) concentrations and water temperature for the June 2022 samples. (d) Isotopic composition of the June 2022 samples.

### Samples collected in August 2022

350

351

352353

354

355

356

357

358

359

360361

362

363364

365

366367

368369

370

371

372

373

375

376

377

PC1 accounts for 60.57 % of the variance in the dataset and is strongly influenced by solute concentrations, with PC scores ranging from 0.47 to 0.48 (Fig. 7a). PC2, which explains 22.34 % of the variance, reflects opposing influences of temperature (0.68) and isotopic composition (-0.63), PC3, accounting for 9.01 % of the variance, shows joint positive correlations with both temperature (0.71) and isotopic composition (0.63). Clustering analysis clearly distinguishes different sample types, forming 9 clusters, the maximum achievable based on the parametrization (Fig. 7b). Cluster 3 consists of glacial outlet samples, characterized by low solute concentrations (16 to 38 mg L<sup>-1</sup> in TDS), cold temperatures (0.06 to 0.07 °C), and depleted isotopic compositions (-21.6 to -22 % vs. VSMOW in  $\delta^{18}$ O) as seen in Figs. 7c and 7d. Clusters 5 and 6 comprise Shar Shaw Tagà River samples, with warmer temperatures (3.47 °C to 6.26 °C), higher solute concentrations (88 to 238 mg L<sup>-1</sup> in TDS), and depleted isotopic compositions (-21.8 to -22.2 ‰ vs. VSMOW in  $\delta^{18}$ O). The distinction between these clusters may be attributed to variations in the glacial regime diurnal cycle and weather conditions based on sampling times. Clusters 4 and 8 include samples from springs near the upper end of the rock glacier front and at the transition area with the ice-debris complex (e.g., S-IDC5, S-RG1, S-RG2). As shown in Figs. 7c and 7d, these springs display high concentrations of mineral elements (209 to 304 mg L<sup>-1</sup> in TDS) and enriched isotopic compositions (-20.6 to -20.9 ‰ vs. VSMOW in δ<sup>18</sup>O). Clusters 2 and 9 are represented by springs S-RG7, S-RG8, S-RG9A, and S-IDC1, which exhibit high but narrow ranges of solute concentrations (282 to 309 mg L<sup>-1</sup> in TDS) and more depleted isotopic compositions  $(-21.6 \text{ to } -21.8 \text{ }\% \text{ vs. VSMOW in } \delta^{18}\text{O})$ , as shown in Fig. 7d. Clusters 1 and 7 include other springs from the N1 subsection of the Shár Shaw Tagà River, which are characterized by low solute concentrations (111 to 162 mg L<sup>-1</sup> in TDS) and enriched isotopic compositions (-20.4 to -20.9 ‰ vs. VSMOW in δ¹8O). Fig. 7d clearly distinguishes samples with depleted isotopic compositions (below -21.5 % vs. VSMOW in  $\delta^{18}$ O) from those with enriched compositions (above -20.9 % vs. VSMOW in  $\delta^{18}O$ ).

In late summer, the hydrochemical signatures of the springs show significant contrasts, with a high number of clusters.

However, springs S-RG7, S-RG8, and S-RG9A share isotopic signatures similar to glacial meltwater from S-G1, S-G2, and

S-G3, indicating a glacial input. Despite being located on opposite sides of the river, these springs cluster together, contrasting

with the other springs. Most of the rock glacier spring samples show very cold temperatures (< 2 °C; Fig. 7c).

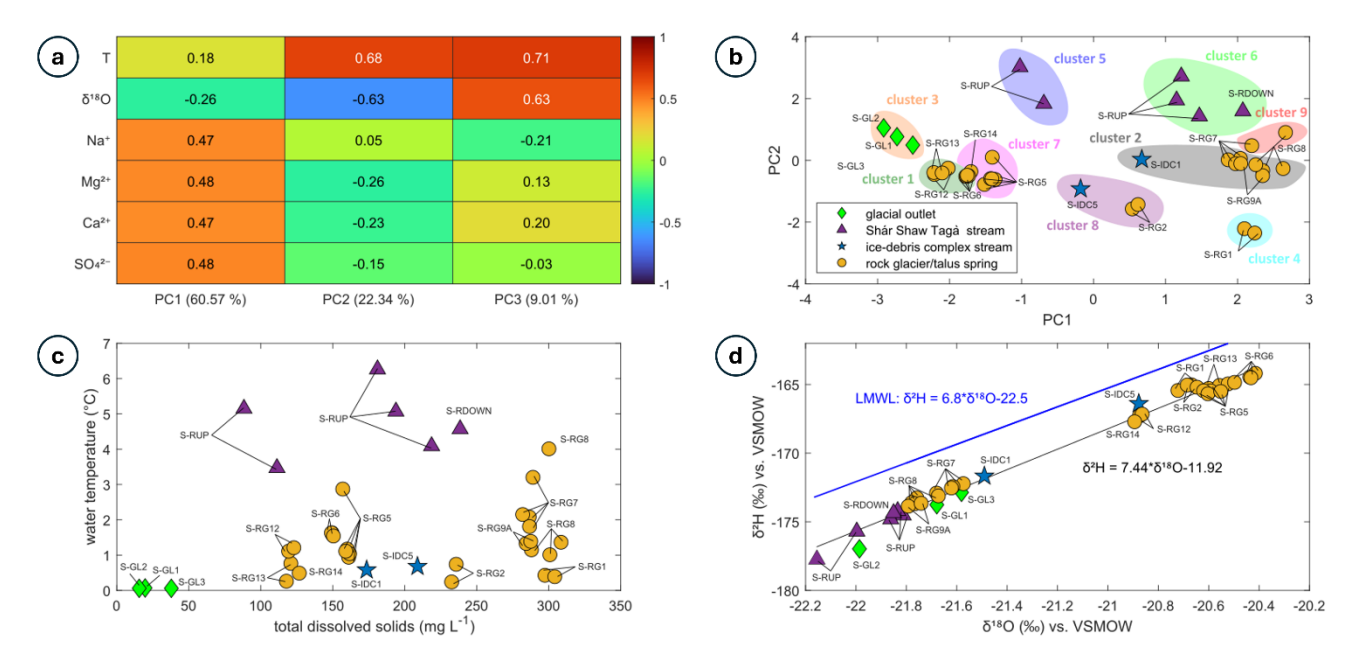


Fig. 7: (a) PCA scores for August 2022 samples. The explained variance for each PC is indicated in the legend of the horizontal axis. (b) Distribution of clusters formed from August 2022 samples following PCA and k-means clustering. Symbols represent different sample types, and ellipses illustrate the distribution of each cluster. (c) Distribution of total dissolved solids (TDS) concentrations and water temperature for the August 2022 samples. (d) Isotopic composition of the August 2022 samples.

# Samples collected in June 2023

PCA conducted on samples collected in June 2023 revealed that PC1 accounts for 68.79 % of the variance (Fig. 8a), primarily driven by solute concentrations (PC scores ranging from 0.40 to 0.48). PC2 and PC3 explain 15.54 % and 10.43 % of the variance, respectively. PC2 is mainly influenced by water temperature (0.88), while PC3 is dominated by isotopic composition (0.86).

The glacier outlet samples form a distinct cluster, labeled as Cluster 3 (Fig. 8b). The remaining samples are divided into two clusters, with a clear distinction based on the maximum number of clusters (5). Cluster 1 consists solely of Shár Shaw Tagà River samples from the upstream part of the N1 subsection. Cluster 2 includes spring samples and Shár Shaw Tagà River samples collected in the downstream part of the N1 subsection. River samples from the downstream N1 subsection and spring samples exhibit higher solute concentrations (from 121 to 147 mg L<sup>-1</sup> in TDS) and colder temperatures (from 0.7 to 4 °C, with 14 out of 16 samples < 2 °C) compared to the upstream N1 samples, which have lower solute concentrations (87 to 125 mg L<sup>-1</sup>) and warmer temperatures (5.3 to 9.5 °C; Fig. 8c). The isotopic composition is generally more enriched for the upstream N1 river samples than for the downstream N1 river and spring samples (Fig. 8d). The isotopic composition of one of the two glacial water samples from G-B1 (sample S-GL1) is similar to the composition from the Shár Shaw Tagà River in upstream N1 (water flowing from G-A1). However, the second S-GL1 sample shows a much more enriched isotopic composition, due

to a two-day interval between the respective samplings. The most enriched sample (-21.2 % vs. VSMOW in  $\delta^{18}$ O and -165.4 % vs. VSMOW in  $\delta^{2}$ H) was taken first, when the G-B1 glacier was still snow-covered. The most depleted sample (-22.4 % vs. VSMOW in  $\delta^{18}$ O and -173.6 % vs. VSMOW in  $\delta^{2}$ H) was taken two days later, following significant snowmelt cover on G-B1 and the initiation of glacial melt.

The springs located on opposite sides of the river along the N1 subsection cluster together and exhibit close hydrochemical signatures, similar to what was observed in August 2022. By distinguishing between two clusters, the PCA highlights the important influence of these springs on the Shár Shaw Tagà River. Their outflows significantly lower the water temperature and increase solute concentrations in the river.

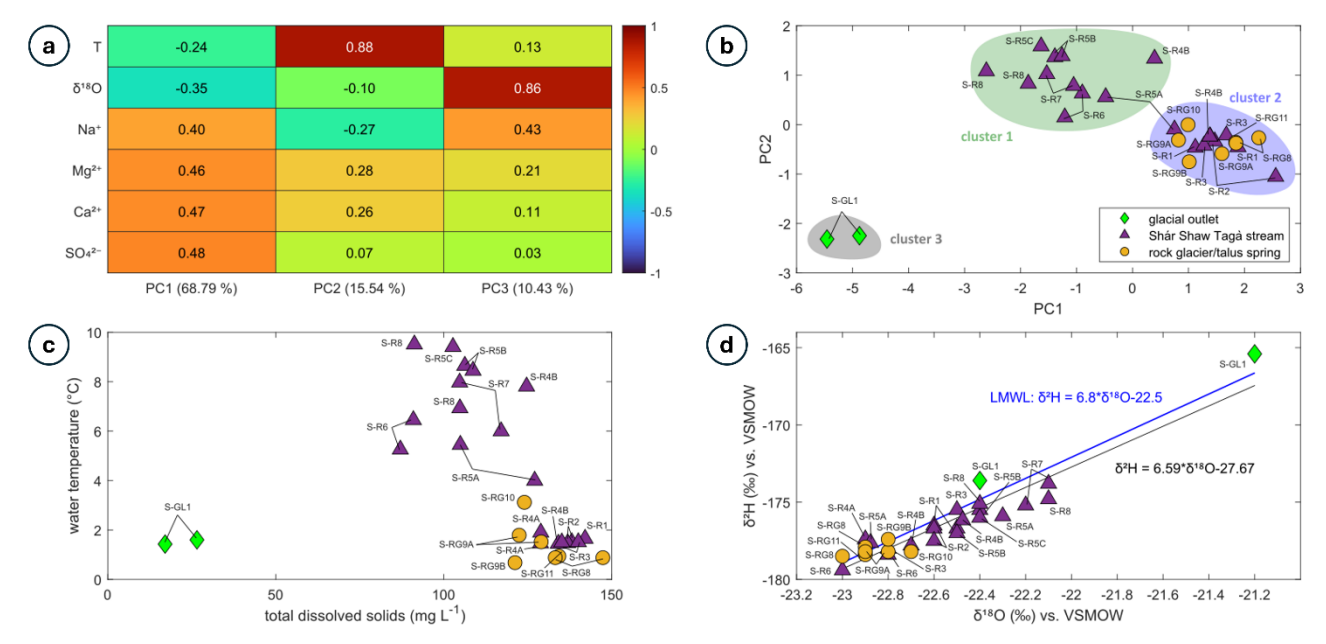


Fig. 8: (a) PCA scores for June 2023 samples. The explained variance for each PC is indicated in the legend of the horizontal axis. (b) Distribution of clusters formed from June 2023 following PCA and k-means clustering. Symbols represent different sample types, and ellipses illustrate the distribution of each cluster. (c) Distribution of total dissolved solids (TDS) concentrations and water temperature for the June 2023 samples. (d) Isotopic composition of the June 2023 samples.

# Synthesis of physico-hydrochemical characterisation

The springs surrounding RG-A1's front exhibit heterogeneous hydrochemical signatures. However, a group of springs along the N1 subsection (S-RG7, S-RG8, and S-RG9A) cluster together in PCA and share high EC values, depleted isotopic compositions, high solute concentrations, and similar radon activities. Despite being located on opposite sides of the river, these three springs show striking similarities, suggesting a common origin. Their isotopic compositions are comparable to those of glacial meltwater sampled at G-B1 and in the Shár Shaw Tagà River, differing significantly from other springs along RG-A1's front. The other springs around RG-A1's front exhibit diverse hydrochemical signatures under varying hydrometeorological conditions. All springs consistently exhibit cold temperatures. During low-discharge periods, such as June

- 421 2023, the springs along the N1 subsection considerably increase downstream solute concentrations and radon activities in the
- Shár Shaw Tagà River, while their cold outflows reduce stream temperature. .

# 4.3 TIR survey

- 424 The TIR survey detected four cold water outflows outside the "narrow section" of the Shár Shaw Tagà River, located in the 425 outwash plain downstream of RG-A1 (Fig. 9). Two outflows were identified on the left bank: one associated with meltwater 426 originating from a snow patch at the front of RG-A1, and the other is from a persistent snow patch on the west flank of the 427 valley. The other two outflows were located on the right bank, originating from the middle of the outwash plain near the front 428 of RG-B2. These four outflows are not supplied by RG-A1, as they originate from snow patches or from the right bank. 429 The furthest downstream exfiltration area in the "narrow section" (TIR-L8) is situated in the N1 subsection, just a few meters 430 upstream of the bedrock outcrop (Fig. 9). Within the N1 subsection, eight groundwater exfiltration areas were identified on 431 the left bank of the main channel, and six on the right bank. Exfiltration areas on the left bank are generally smaller, with
- plume lengths ranging from 1 to 6 m, four of these less than 2 m long. In contrast, exfiltration areas on the right bank are larger, with plume lengths ranging from 5 to 14 m, and four exceed 10 m in length. These exfiltration areas were clearly visible as
- color contrasts, distinguishing the warmer surface waters from the colder groundwater exfiltrations (Fig. 10a). The positions
- of the mixing plumes were observed at each location. In the most notable exfiltration areas (plume lengths > 2 m), clearer
- 436 water was observed in the visible video footage, facilitating the validation of groundwater exfiltration detection (Fig. 10b).
- Two of the six groundwater exfiltration areas detected from the right bank can be associated with springs sampled and
- 438 measured during the 2022 and 2023 campaigns for physico-hydrochemical analysis (TIR-R2 and TIR-R3 correspond to S-
- RG9A and S-RG9B, respectively). As mentioned in Sect. 2, depending on the river level and meteorological conditions, the
- outflow locations of the springs on the left side of the river have been observed to shift 10 to 20 m downstream of the RG-A1
- front. During the TIR survey, these conditions were met, and no exfiltration area was found directly at the location of a spring
- sampled in 2022 and 2023. Instead, exfiltration areas on the left bank were detected 20 m downstream of their corresponding
- springs sampled earlier. Therefore, exfiltration areas TIR-L1, TIR-L2 and TIR-L8 can be associated with the springs S-RG8,
- S-RG10 and S-RG11, respectively (Fig. 9).
- The drone-based TIR survey identified a high density of cold groundwater exfiltrations from both the left and right banks of
- the N1 subsection of the Shár Shaw Tagà River, upstream of the bedrock outcrop. Exfiltration areas on the right bank exhibited
- longer plumes, suggesting higher discharge. Two cold outflows were detected in the downstream outwash plain on the left
- bank, but no groundwater origin was identified for these.

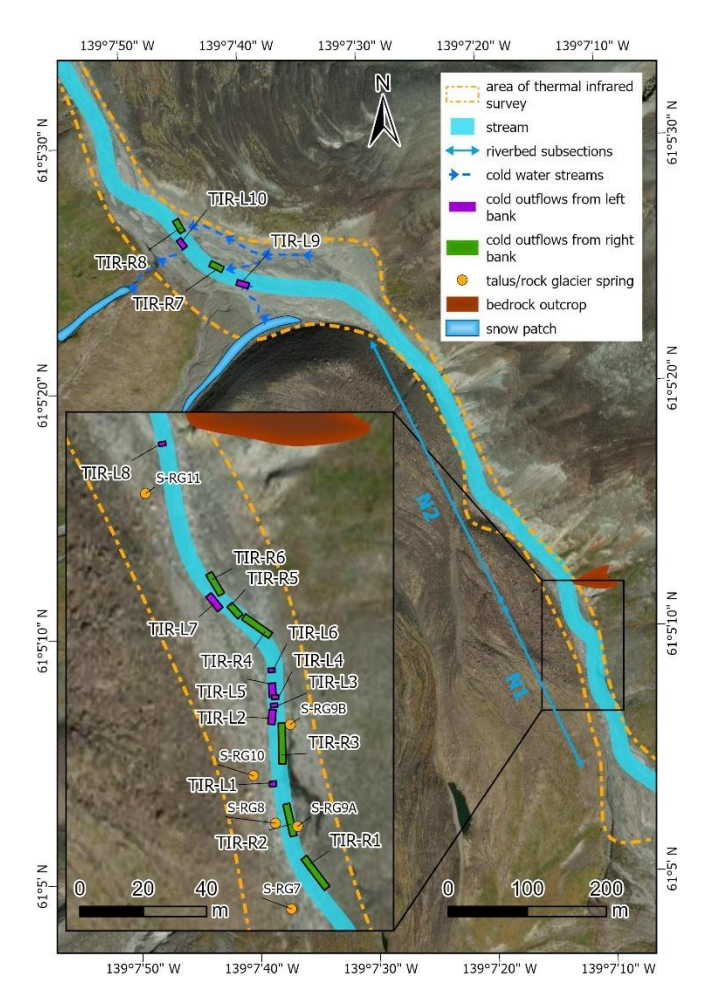


Fig. 9: Location of cold water outflows detected by the TIR survey along the Shár Shaw Tagà riverbed. The zoomed-in view of the "narrow section" highlights an area with a high density of cold groundwater outflows detected on both sides of the river, upstream of a bedrock outcrop constraining the riverbed. Additional cold water outflows are observed in the downstream outwash plain, originated from either snow patch melt on the left side or from the right bank of the outwash plain. Springs that outflow from RG-A1 or the opposite talus slope and were sampled during the 2022 and 2023 campaigns are marked in the zoomed-in panel. Basemap credits: Esri.

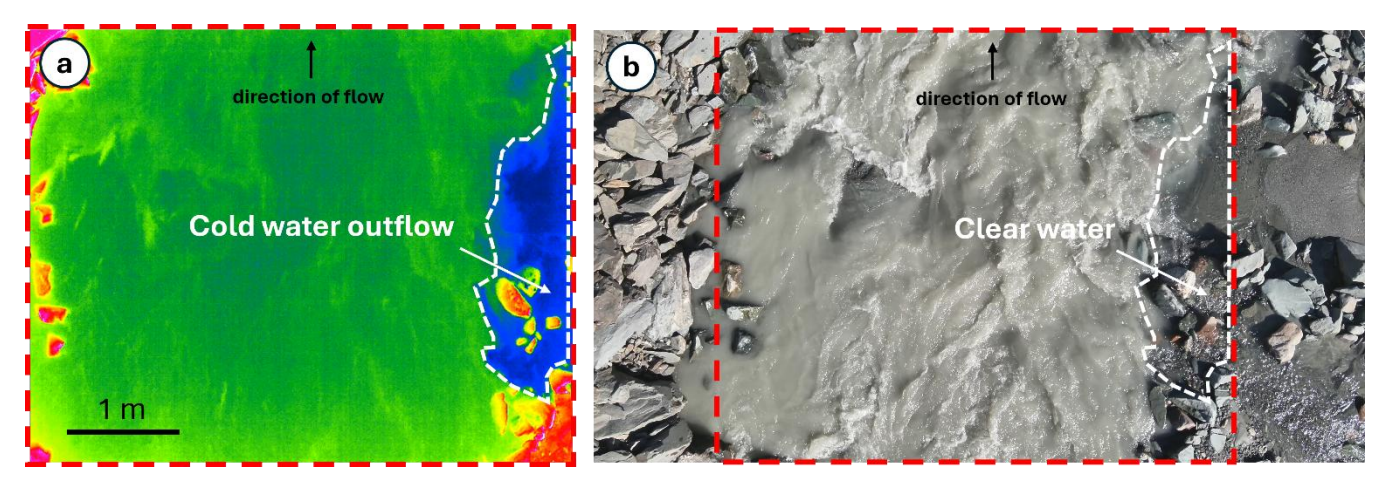


Fig. 10: (a) TIR capture showing cold groundwater outflow (in blue, delimited by the dashed white line), mixing with the warmer waters of the Shár Shaw Tagà River (in green) at the TIR-R2 location. Note that the video does not provide a color scale. (b) RGB image capture showing clear water outflowing into the Shár Shaw Tagà River, which is characterized by a significant sediment load at the TIR-R2 location. The cold water area detected with TIR is delimited by the dashed white line. The extent of the TIR capture is indicated by the dashed red line. Flight data and information can be accessed as Supplemental Material in Charonnat and Baraer, 2025.

# 5 DISCUSSION

# 5.1 The rock glacier forces resurgence of shallow groundwater flow

The preliminary inventory of springs and the TIR survey identified a high density of spring outflows from both banks of the N1 subsection of the Shár Shaw Tagà River. The physico-hydrochemical characterization indicates that the springs on both banks share a similar signature originating from glacial melt, suggesting a common source (Fig. 7 and 8). The contribution of internal ice melt in rock glacier outflows is known to be minimal and does not significantly influence isotopic signatures (Croce and Milana, 2002; Krainer and Mostler, 2002; Krainer et al., 2007). This evidence supports the conclusion that these springs are fed by groundwater of glacial origin. In June 2023, a low-discharge period, field observations revealed river water losses before entering the upstream outwash plain, where the riverbed temporarily lacked surface flow. Surface flow resumed only from the N1 subsection due to groundwater inflows, pointing to the existence of shallow subsurface flow through the upstream outwash plain. Together, these elements indicate that water outflowing from the springs along the N1 subsection resurges from lateral shallow groundwater, likely infiltrating through the riverbed and flowing within the lateral alluvial aquifer before resurfacing.

Contrary to initial hypotheses, no evidence was found of outflow originating from the head of the rock glacier's subcatchment

Contrary to initial hypotheses, no evidence was found of outflow originating from the head of the rock glacier's subcatchment (comprising glaciers G-B1 and G-B2). Instead, the physico-hydrochemical characterization suggests that glacial meltwater entering the water to the river derives from upstream outwash plains of the main Shár Shaw Tagà catchment. In contrast, the other springs emerging at the front of the rock glacier appear to be linked to internal drainage systems within the rock glacier itself. These springs are primarily fed by snowmelt in the early season and by summer precipitation later in the season, with

minimal or negligible glacier melt contribution, as shown by the physico-hydrochemical characterization of the samples collected in June 2022 and August 2022, respectively. Across Canada, precipitation is typically enriched in heavy isotopes during the snow-free period and depleted during winter and spring (Gibson et al., 2020). Accordingly, the depleted isotopic compositions, low solute concentrations, and cold temperatures measured in early June point to a snowmelt origin, while the enriched isotopic compositions in August reflect a stronger influence from rainfall. This seasonal distinction is further supported by contrasting results from springs in the N1 subsection, which exhibit characteristics of both groundwater and glacier-fed sources. Some springs likely reflect a mix of these sources, with their physicochemical parameters and clustering reflecting these dual influences depending on hydro-meteorological conditions and time periods.

Parafluvial flow is common in outwash plains with coarse-grained unconsolidated sediments, occurring in river reaches where water is lost before rejoining the river in gaining reaches (Cartwright and Hofmann, 2016). Outwash plains, often underlain by bedrock, retaining groundwater in the shallow subsurface, providing baseflow during dry periods when upstream discharge is limited (Müller et al., 2024). Fractured and faulted bedrock aquifers can further contribute to baseflow in outwash plains (Hayashi, 2019; Müller et al., 2022). In this case, the resurgence of parafluvial and shallow groundwater flow is visible during dry periods. The dynamic location of the springs reported between sampling campaigns reflects the lateral and vertical extent of the alluvial aquifer. The lower density of springs identified beyond the bedrock outcrop at the end of the N1 subsection suggests a shallow bedrock interface with limited groundwater flow capacity. Additionally, the faults inferred along the riverbed in previous geological studies (Dodds and Campbell, 1992) may facilitate groundwater flow from outwash plains upstream of the rock glacier to the N1 subsection, where it is forced to resurge.

The cold temperatures measured in the springs of the N1 subsection indicate that outflows from the alluvial aquifer are cooled by adjacent frozen content, such as massive ice or permafrost (e.g. Carturan et al., 2016). Frozen content has been confirmed in the rock glacier by Evin et al. (1997), and is suspected for the talus slope, based on Scapozza, (2015). The frozen content on both sides of the Shár Shaw Tagà River constrains the alluvial aquifer, forcing groundwater to resurface through springs and cold water upwellings in the riverbed. The advance of the rock glacier, which considerably narrows the riverbed, further enforces this constraint. The younger lobes of the rock glacier, potentially containing higher amounts of frozen content, extend north from the bedrock outcrop to the downstream outwash plain, possibly acting as an additional barrier to groundwater flow where they border the Shár Shaw Tagà River. Thus, the location of the resurgences in the N1 subsection can be explained by the geomorphic properties of the rock glacier. The narrowing of the riverbed by the rock glacier's advance and the presence of frozen content constrain the riverbed, forcing the resurgence of shallow groundwater flow.

# 5.2 The rock glacier affects downstream cryo-hydrological processes and hydrological continuity

The proximity of bedrock and ground ice in the narrow section of the Shár Shaw Tagà River critically reduces the width and depth of the alluvial aquifer, leading to groundwater exfiltrations along the N1 subsection, as discussed in Sect. 5.1. Aufeis typically develop in areas where river flow velocity decreases, such as braided channels and outwash plains (Hu and Pollard,

1997). The TL monitoring suggests that the resurgences from the alluvial aquifer provide the water from the N1 subsection but the decrease in river flow velocity and channel depth creates conditions favourable for the formation of aufeis in the outwash plain immediately downstream of the rock glacier. In contrast, the steeper slope in the N1 subsection likely inhibits aufeis formation directly at the springs locations. Thus, the rock glacier plays a significant role in influencing downstream cryo-hydrological processes.

The high density of springs along the N1 subsection and their distinct physicochemical signatures substantially affect the downstream Shár Shaw Tagà River. The solute enrichment observed in these springs is attributed to water-rock interactions along groundwater flow paths. Prolonged residence time in aquifers facilitates the accumulation of dissolved solutes (Hem, 1985). In addition, the springs may be partially connected to internal drainage systems within the rock glacier, which are known to generate solute-rich outflows (Colombo et al., 2018). Lastly, the proximity to buried ground ice and permafrost – both within the rock glacier and in adjacent talus slopes – may enhance the release of mineral elements through thermal erosion of the ice-sediment matrix (Jones et al., 2019). The physico-hydrochemical characterization from June 2023 demonstrates that during dry periods, these springs notably increase solute concentrations and radon activities, while simultaneously cooling the river water. These findings are consistent with prior studies showing the influence of rock glaciers on the physicochemical characteristics of downstream surface waters (e.g., Bearzot et al., 2023; Brighenti et al., 2023; Robinson et al., 2022; Wagner et al., 2021). However, the rock glacier in this study alters the entire riverbed and its physicochemical parameters primarily due to its geomorphic properties. Contrary to initial hypotheses based on early observations and the literature, its internal hydrological behavior does not account for the critical impact the rock glacier has on the riverbed's hydrological system.

# 5.3 Future evolution of the rock glacier influence on catchment hydrology

Predicting the future evolution of the system described in Sect. 5.1 and 5.2 is challenging. However, several scenarios across different timescales can be envisioned. Frozen content is likely to persist in depositional landforms for extended periods, as residual ice has been detected in rock glaciers below the modeled elevation limit in multiple cases (e.g., Carturan et al., 2024; Colucci et al., 2019). Future hydrological conditions in alpine catchments will likely be characterized by a reduced hydrological influence of glaciers, lower discharge and an increased contribution from groundwater and periglacial features to streamflow (Huss et al., 2017; Jones et al., 2019; Zierl and Bugmann, 2005). These conditions were observed during the June 2023 sampling campaign, which occurred after the peak of snowmelt and prior to the peak of glacial ablation, leading to a substantial influence of groundwater resurgences on the Shár Shaw Tagà River. Similar conditions may be expected in the future, with groundwater outflows caused by the rock glacier expected to gain influence in the Shár Shaw Tagà River. However, the degradation of frozen content around the riverbed may alter this scenario, as rising air temperatures continue to drive permafrost thaw. Additionally, thermal and mechanical erosion caused by lateral groundwater flow could expand the parafluvial zone and create alternative subsurface flow paths, reducing the hydrological discontinuity and disruptive effects of the rock glacier.

The absence of evident streamflow contribution from the G-B1 subcatchment to the Shár Shaw Tagà River, as highlighted in Sect. 5.1, suggests substantial deep infiltration of surface and shallow groundwater flow between the glaciers of the subcatchment and the rock glacier. Although the role of rock glaciers in deep infiltration has not been thoroughly documented to our knowledge, it is suggested that their high vertical and horizontal flow transmissivity may enhance infiltration into deep aquifers and groundwater recharge (Navarro et al., 2023). From a broader perspective, it is considered that deep groundwater systems link mountain cryosphere components to lowlands aquifers through mountain-block recharge (van Tiel et al., 2024). In this context, increased infiltration due to glacial retreat and permafrost degradation may position rock glaciers and other depositional features as critical hubs in proglacial areas, contributing to regional groundwater circulation and water resources.

# 5.4 Limitations and perspectives

545

546

547

548

549

550

551

552

553

554

555

556

557

558

559

560

561

562

563

564

565

566

567

568

569

570

571

572

573

The physico-hydrochemical characterization conducted in this study was based on three sampling campaigns under varying hydro-meteorological conditions. These diverse settings posed several challenges for water sampling, including issues with accessibility, safety concerns, periods of no flow, and the need to prioritize specific areas. As a result, some sampling sites could not be revisited during every campaign, leading to gaps in the data over time. Moreover, fluctuating weather conditions during a single campaign in proglacial environments likely contributed to variations in physicochemical parameters at some sites. Where possible, multiple samples were taken at different times or on different days within the same campaign to minimize biases caused by diurnal and meteorological variations. Consequently, some sites could not be compared across campaigns, and their characterization can remain incomplete. On the other hand, these challenges allowed us to identify the varying influences of different drainage systems on certain springs. Upon initial observations and hypotheses, we adopted a unique multi-method approach, which evolved as we refined our understanding of the system. While this combination of methods was crucial in addressing the research question and drawing the conclusions presented, alternative approaches could have provided a more direct route to the findings. Future research could build on the insights gained in this study by investigating the hydrological roles of other rock glaciers within the same valley or in different regions. Such studies would help assess whether similar patterns occur across varying settings. Moreover, this research underscores the potential role of the rock glacier and adjacent depositional features in facilitating the infiltration of water into deep groundwater systems, as suggested by the lack of water outflow from the head of the subcatchment to the

### 6 CONCLUSIONS

574 The geomorphic properties of rock glaciers make them dynamic features capable of altering riverbed hydrological systems.

resource supply during deglaciation. The authors strongly encourage further works in this direction.

As assessed in this study, rock glaciers can obstruct proglacial outwash plains, thereby controlling and constraining shallow

the Shár Shaw Tagà River. Characterizing these transfers is crucial for understanding the role of proglacial areas in water

587

588 589

590

groundwater flow. This obstruction results in channel confinement, which induces resurgences from the alluvial aquifer, with profound impacts on both the hydrochemistry and hydrogeomorphology of alpine catchments. Rock glacier disruption leads to substantial changes in the physicochemical parameters of streamflow, and contributes to the formation of aufeis, a consequence not previously documented in the literature. In contrast to initial hypotheses, the internal hydrological system of the rock glacier does not exhibit a significant influence on downstream surface waters. Instead, the critical disruption to the riverbed hydrological system is due to the geomorphic constraint imposed by the rock glacier on the alluvial aquifer. The water that flows from the subcatchment above the rock glacier is suspected to infiltrate deep groundwater systems through the rock glacier and the adjacent depositional features, as it could not be traced beyond the rock glacier. Thus, this study emphasizes the complexity and potentially misleading nature of characterizing groundwater flow pathways in proglacial environments. The findings also have broader implications for mountain hydrology and water resources, highlighting the importance of rock glaciers and proglacial systems as critical hydrological features and potential hubs for mountain-block recharge, linking the mountain cryosphere to deep groundwater systems.

Appendix: Table A1

| Sampling sites | Northing<br>(UTM) | Easting (UTM) | Elevation (m a.s.l.) | Comments                              | Dates and times of sampling |             |                                  |
|----------------|-------------------|---------------|----------------------|---------------------------------------|-----------------------------|-------------|----------------------------------|
|                |                   |               |                      |                                       | June 2022                   | August 2022 | June 2023                        |
| S-R1           | 6773938           | 601332        | 1738                 | Shár Shaw Tagà river (narrow section) | NV                          | NV          | 15/06/23 12:50<br>16/06/23 13:00 |
| S-R2           | 6773933           | 601336        | 1739                 | Shár Shaw Tagà river (narrow section) | NV                          | NV          | 15/06/23 13:07<br>16/06/23 13:10 |
| S-R3           | 6773933           | 601336        | 1739                 | Shár Shaw Tagà river (narrow section) | NV                          | NV          | 15/06/23 13:25<br>16/06/23 13:40 |
| S-R4A          | 6773813           | 601409        | 1741                 | Shár Shaw Tagà river (narrow section) | NV                          | NV          | 15/06/23 13:50                   |
| S-R4B          | 6773817           | 601408        | 1746                 | Shár Shaw Tagà river (narrow section) | NV                          | NV          | 15/06/23 14:35<br>16/06/23 14:20 |
| S-R5A          | 6773817           | 601408        | 1746                 | Shár Shaw Tagà river (narrow section) | NV                          | NV          | 15/06/23 14:40<br>16/06/23 15:10 |
| S-R5B          | 6773817           | 601408        | 1746                 | Shár Shaw Tagà river (narrow section) | NV                          | NV          | 15/06/23 14:10<br>16/06/23 15:25 |
| S-R5C          | 6773781           | 601407        | 1747                 | Shár Shaw Tagà river (narrow section) | NV                          | NV          | 16/06/23 14:45                   |

| 6773685  | 601449  | 1759  | Shár Shaw Tagà river (narrow  | NV   | NV   | 15/06/23 16:40  |
|----------|---|---|---|--|--|---|
|          |   |   | <i>'</i>  |  |  | 16/06/23 15:45  |
| 6773691  | 601445  | 1753  | - '   | NV   | NV   | 15/06/23 16:50  |
|          |   |   | ,   |  |  | 16/06/23 16:00  |
| 6773691  | 601445  | 1753  | Shár Shaw Tagà river (narrow  | NV   | NV   | 15/06/23 17:00  |
|          |   |   | section)  |  |  | 16/06/23 16:10  |
| 6774302  | 600936  | 1687  | Shár Shaw Tagà river (downstream floodplain)  | NV   | 19/08/22 13:05   | NV  |
| 6773641  | 601455  | 1749  | Shár Shaw Tagà river (upstream  | NV   | 16/08/22 12:00   | NV  |
|          |   |   | floodplain)   |  | 16/08/22 16:16   |   |
|          |   |   |   |  | 17/08/22 13:12   |   |
|          |   |   |   |  | 18/08/22 12:35   |   |
|          |   |   |   |  | 19/08/22 13:01   |   |
| 6772289  | 600889  | 2083  | stream at G-B1 snout  | NV   | 18/08/22 18:36   | 19/06/23 14:35  |
|          |   |   |   |  |  | 21/06/23 12:05  |
| 6772230  | 600819  | 2109  | stream at G-B1 snout  | NV   | 18/08/22 18:06   | NV  |
|          |   |   |   |  |  |   |
| 6772239  | 600703  | 2086  | stream at G-B1 snout  | NV   | 18/08/22 19:03   | NV  |
|          |   |   |   |  |  |   |
| 6772896  | 600330  | 1886  | ice-debris complex stream   | 16/06/22 15:56   | 18/08/22 20:29   | NV  |
|          |   |   |   | 18/06/22 17:50   |  |   |
| 6772897  | 600330  | 1886  | ice-debris complex stream   | 18/06/22 17:56   | NV   | NV  |
|          |   |   |   |  |  |   |
| 6772943  | 600345  | 1891  | ice-debris complex stream   | 16/06/22 15:37   | NV   | NV  |
|          |   |   |   |  |  |   |
| 6772967  | 600379  | 1893  | ice-debris complex stream   | 16/06/22 17:04   | NV   | NV  |
|          |   |   |   |  |  |   |
| 6773216  | 600703  | 1860  | ice-debris complex stream   | 16/06/22 17:40   | 18/08/22 20:55   | NV  |
|          |   |   |   |  |  |   |
| 6773340  | 601180  | 1797  | spring at RG-A1 front   | NV   | 17/08/22 11:58   | NV  |
|          |   |   |   |  | 18/08/22 13:52   |   |
| 6773415  | 601279  | 1780  | spring at RG-A1 front   | 12/06/22 16:54   |  | NF  |
| 0113413  | 001279  | 1700  | Spring at RO-AT HOIR  |  |  | 171   |
| (772 442 | (01270  | 1770  | I PO A1 C   |  |  | NE  |
| 67/3442  | 601378  | 17/0  | spring at RG-A1 front   | 19/06/22 14:48   | NF   | NF  |
|          | 601414  | 1770  | spring at RG-A1 front   | 19/06/22 13:52   | NF   | NF  |
|          | 6773691<br>6773691<br>6773691<br>6774302<br>6773641<br>6772289<br>6772230<br>6772239<br>6772239 | 6773691       601445         6773691       601445         6774302       600936         6773641       601455         6772289       600889         6772230       600819         6772239       600703         6772896       600330         6772943       600345         6773216       600703         6773340       601180         6773415       601279 | 6773691       601445       1753         6773691       601445       1753         6774302       600936       1687         6773641       601455       1749         6772289       600889       2083         6772230       600819       2109         6772239       600703       2086         6772896       600330       1886         6772943       600345       1891         6773216       600703       1860         6773340       601180       1797         6773415       601279       1780 | 6773691         601445         1753         Shár Shaw Tagà river (narrow section)           6773691         601445         1753         Shár Shaw Tagà river (narrow section)           6773691         601445         1753         Shár Shaw Tagà river (narrow section)           6774302         600936         1687         Shár Shaw Tagà river (downstream floodplain)           6773641         601455         1749         Shár Shaw Tagà river (upstream floodplain)           6772289         600889         2083         stream at G-B1 snout           6772230         600819         2109         stream at G-B1 snout           6772294         600703         2086         stream at G-B1 snout           6772896         600330         1886         ice-debris complex stream           6772897         600330         1886         ice-debris complex stream           6772943         600345         1891         ice-debris complex stream           6772967         600379         1893         ice-debris complex stream           6773216         600703         1860         ice-debris complex stream           6773340         601180         1797         spring at RG-A1 front           6773415         601279         1780         spring at RG-A1 front | 6773691         601445         1753         Shar Shaw Tagà river (narrow section)         NV           6773691         601445         1753         Shar Shaw Tagà river (narrow section)         NV           6773691         601445         1753         Shar Shaw Tagà river (narrow section)         NV           6774302         600936         1687         Shar Shaw Tagà river (downstream floodplain)         NV           6773641         601455         1749         Shar Shaw Tagà river (upstream floodplain)         NV           6772289         600889         2083         stream at G-B1 snout         NV           6772230         600819         2109         stream at G-B1 snout         NV           6772289         600330         1886         ice-debris complex stream         16/06/22 15:56 18/06/22 17:50           6772897         600330         1886         ice-debris complex stream         18/06/22 17:56           6772943         600345         1891         ice-debris complex stream         16/06/22 17:04           6773216         600379         1893         ice-debris complex stream         16/06/22 17:04           6773340         601180         1797         spring at RG-A1 front         NV           6773415         601279         1780 | 6773691         601445         1753         Shár Shaw Tagà river (narrow section)         NV         NV           6773691         601445         1753         Shár Shaw Tagà river (narrow section)         NV         NV           6773691         601445         1753         Shár Shaw Tagà river (downstream floodplain)         NV         19/08/22 13:05           6774302         600936         1687         Shár Shaw Tagà river (downstream floodplain)         NV         16/08/22 12:00           6773641         601455         1749         Shár Shaw Tagà river (upstream floodplain)         NV         16/08/22 13:12 18:06           6772289         600889         2083         stream at G-BI snout         NV         18/08/22 18:36           6772230         600703         2086         stream at G-BI snout         NV         18/08/22 18:06           6772289         600330         1886         ice-debris complex stream         16/06/22 15:56         NV           6772897         600330         1886         ice-debris complex stream         18/06/22 17:50         NV           6772943         600345         1891         ice-debris complex stream         16/06/22 17:04         NV           6773216         600703         1860         ice-debris complex stream         16/06/22 |

| S-RG5  | 6773643 | 601423 | 1770 | spring at RG-A1 front              | 19/06/22 13:45 | 16/08/22 11:30 | NV             |
|--------|---------|--------|------|------------------------------------|----------------|----------------|----------------|
|        |         |        |      |                                    |                | 16/08/22 16:04 |                |
|        |         |        |      |                                    |                | 17/08/22 12:44 |                |
|        |         |        |      |                                    |                | 18/08/22 12:47 |                |
|        |         |        |      |                                    |                | 19/08/22 13:46 |                |
| S-RG6  | 6773683 | 601421 | 1758 | spring at RG-A1 front              | 19/06/22 13:30 | 16/08/22 12:40 | NV             |
|        |         |        |      |                                    |                | 17/08/22 13:05 |                |
|        |         |        |      |                                    |                | 18/08/22 12:27 |                |
|        |         |        |      |                                    |                | 19/08/22 13:24 |                |
| S-RG7  | 6773736 | 601413 | 1746 | spring at RG-A1 front              | 19/06/22 13:18 | 16/08/22 13:05 | NV             |
|        |         |        |      |                                    |                | 17/08/22 13:58 |                |
|        |         |        |      |                                    |                | 18/08/22 12:14 |                |
|        |         |        |      |                                    |                | 19/08/22 13:12 |                |
| S-RG8  | 6773763 | 601408 | 1744 | spring at RG-A1 front              | 19/06/22 12:50 | 16/08/22 13:15 | 15/06/23 14:55 |
|        |         |        |      |                                    |                | 17/08/22 14:13 | 16/06/23 14:35 |
|        |         |        |      |                                    |                | 18/08/22 11:11 |                |
|        |         |        |      |                                    |                | 19/08/22 12:34 |                |
| S-RG9A | 6773762 | 601415 | 1752 | spring flowing from talus opposite | NV             | 16/08/22 12:13 | 15/06/23 14:55 |
|        |         |        |      | to RG-A1 front (right bank)        |                | 17/08/22 13:29 | 16/06/23 14:25 |
| S-RG9B | 6773931 | 601335 | 1734 | spring from talus opposite to RG-  | NV             | NV             | 16/06/23 14:10 |
|        |         |        |      | A1 front (right bank)              |                |                |                |
| S-RG10 | 6773778 | 601401 | 1749 | spring at RG-A1 front              | 19/06/22 12:43 | NV             | 16/06/23 14:00 |
| S-RG11 | 6773867 | 601367 | 1738 | spring at RG-A1 front              | 19/06/22 12:35 | NV             | 16/06/23 13:30 |
| S-RG12 | 6773971 | 601281 | 1726 | and a st DC A1 front               | NV             | 18/08/22 11:56 | NV             |
|        | 0//39/1 | 001281 | 1/20 | spring at RG-A1 front              | IN V           | 19/08/22 12:10 | IN V           |
|        |         |        |      |                                    |                |                |                |
| S-RG13 | 6773995 | 601265 | 1726 | spring at RG-A1 front              | NV             | 16/08/22 13:47 | NV             |
|        |         |        |      |                                    |                | 18/08/22 11:40 |                |
| S-RG14 | 6774166 | 601183 | 1712 | spring at RG-A1 front              | 15/06/22 15:30 | 19/08/22 12:30 | NV             |
|        |         |        |      |                                    | 19/06/22 14:25 |                |                |
| S-RG15 | 6774210 | 600985 | 1683 | spring at RG-A1 front              | 19/06/22 15:17 | NV             | NV             |
| S-RG16 | 6774034 | 600854 | 1740 | spring at RG-A1 front              | 19/06/22 15:42 | NV             | NV             |

Table A1: List and description of sites sampled during the three campaigns between June 2022 and August 2023, with UTM coordinates, elevation, dates and times of sampling. Samples are categorized into four distinct types: glacial outlets from the G-B1 glacier snout (S-GL#), ice-debris complex streams in the proglacial area between the glacier tongue and rock glaciers (S-IDC#), Shár Shaw Tagà River (S-R#), and springs from RG-A1 rock glacier front and opposite talus (S-RG#). Sites were not all sampled for every campaign, due to diverse reasons (access and safety issues, no flow, campaign dedicated to a specific area, etc.). When possible,

596 sites were sampled several times to trace potential fluctuations in their physico-chemical signature. When not sampled, the comment 597 "NV" stands for "not visited." The comment "NF," for "no flow," indicates a site not sampled as it was dry when visited. 598 599 Code/Data availability 600 The data supporting this study are available upon request to the corresponding author. 601 602 Video supplement The videos and flight data used for the TIR analysis are available as Supplemental Material in Charonnat and Baraer, 2025, on 603 604 Borealis dataverse (https://doi.org/10.5683/SP3/O57OMY). 605 606 **Author contribution** 607 Conceptualization: B.C. and M.B. Data curation: B.C. Formal analysis: B.C., M.B., J.M.-D. and C.M. Funding acquisition: 608 M.B. and J.M.M. Investigation: B.C., M.B., E.V., J.M.-D., K.W. and E.D. Methodology: B.C., M.B., E.V. and J.M.-D. Project 609 administration: B.C., M.B., E.V. and J.M.-D. Supervision: M.B., J.M.-D. and J.M.M. Visualization: B.C. and K.W. Writing -610 original draft preparation: B.C. Writing - review & editing: B.C., M.B., E.V., J.M.-D., C.M., K.W., E.D. and J.M.M. All 611 authors have read and agreed to the published version of the manuscript. 612 613 **Competing interests** 614 The authors declare that they have no conflict of interest. 615 Acknowledgements 616 We are grateful to the Kluane First Nation and the White River First Nation for the opportunity to conduct research on their 617 territory. We thank the Arctic Institute of North America and the University of Calgary for providing us service and access to 618 their facilities at Kluane Lake Research Station. We thank Parks Canada for their collaboration and for issuing permits that 619 allowed us to conduct research within Kluane National Park and Reserve. 620 621 Financial support 622 This research was supported by the Natural Sciences and Engineering Research Council of Canada, grant numbers RGPIN-623 2020-05612 and RGPNS-2020-05612, and by Natural Resources Canada—Polar Continental Shelf Program, grant number 624 62723. Additional funding for the expedition was provided by the Research Centre on the Dynamics of the Earth System

625

(GEOTOP).

### 626 References

- 627 Abolt, C., Caldwell, T., Wolaver, B., and Pai, H.: Unmanned aerial vehicle-based monitoring of groundwater inputs to surface
- waters using an economical thermal infrared camera, Optical Engineering, 57(05), 1, https://doi.org/10.1117/1.oe.57.5.053113,
- 629 2018.
- 630 Antonelli, M., Klaus, J., Smettem, K., Teuling, A. J., and Pfister, L.: Exploring Streamwater Mixing Dynamics via Handheld
- 631 Thermal Infrared Imagery, Water, 9(5), Article 5, https://doi.org/10.3390/w9050358, 2017.
- 632 Arenson, L. U., Harrington, J. S., Koenig, C. E. M., and Wainstein, P. A.: Mountain Permafrost Hydrology—A Practical
- Review Following Studies from the Andes, Geosciences, 12(2), Article 2, https://doi.org/10.3390/geosciences12020048, 2022.
- 634 Arenson, L., Hoelzle, M., and Springman, S.: Borehole Deformation Measurements and Internal Structure of Some Rock
- Glaciers in Switzerland, Permafrost and Periglacial Processes, 13, 117–135, https://doi.org/10.1002/ppp.414, 2002.
- Baker, E. A., Lautz, L. K., Kelleher, C. A., and McKenzie, J. M.: The importance of incorporating diurnally fluctuating stream
- 637 discharge in stream temperature energy balance models, Hydrological Processes, 32(18), 2901–2914,
- 638 https://doi.org/10.1002/hyp.13226, 2018.
- 639 Baraer, M., McKenzie, J., Bury, J., and Knox, S.: Characterizing contributions of glacier melt and groundwater during the dry
- 640 season in a poorly gauged catchment of the Cordillera Blanca (Peru), Advances in Geosciences, 22, 41-49,
- 641 https://doi.org/10.5194/adgeo-22-41-2009, 2009.
- Baraer, M., McKenzie, J., Mark, B. G., Gordon, R., Bury, J., Condom, T., Gomez, J., Knox, S., and Fortner, S. K.: Contribution
- of groundwater to the outflow from ungauged glacierized catchments: A multi-site study in the tropical Cordillera Blanca,
- 644 Peru, Hydrological Processes, 29(11), Article 11, https://doi.org/10.1002/hyp.10386, 2015.
- Barclay, J. R., Briggs, M. A., Moore, E. M., Starn, J. J., Hanson, A. E. H., and Helton, A. M.: Where groundwater seeps:
- Evaluating modeled groundwater discharge patterns with thermal infrared surveys at the river-network scale, Advances in
- 647 Water Resources, 160, 104108, https://doi.org/10.1016/j.advwatres.2021.104108, 2022.
- Barsch, D.: Rockglaciers: Indicators for the present and former geoecology in high mountain environments, 1996.
- 649 Bearzot, F., Colombo, N., Cremonese, E., di Cella, U. M., Drigo, E., Caschetto, M., Basiricò, S., Crosta, G. B., Frattini, P.,
- 650 Freppaz, M., Pogliotti, P., Salerno, F., Brunier, A., and Rossini, M.: Hydrological, thermal and chemical influence of an intact
- 651 rock glacier discharge on mountain stream water, Science of The Total Environment, 876, 162777,
- 652 https://doi.org/10.1016/j.scitotenv.2023.162777, 2023.
- 653 Birks, S. J., Edwards, T. W. D., Gibson, J. J., Drimmie, R. J. and Michel, F. A.: Canadian network for isotopes in Precipitation,
- 654 http://www.science.uwaterloo.ca/~twdedwar/cnip/cniphome.html, 2004.
- 655 Blöthe, J. H., Rosenwinkel, S., Höser, T., and Korup, O.: Rock-glacier dams in High Asia, Earth Surface Processes and
- 656 Landforms, 44(3), 808–824, <a href="https://doi.org/10.1002/esp.4532">https://doi.org/10.1002/esp.4532</a>, 2019.

- 657 Bodin, X., Schoeneich, P., Deline, P., Ravanel, L., Magnin, F., Krysiecki, J.-M., and Echelard, T.: Le permafrost de montagne
- 658 et les processus géomorphologiques associés: Évolutions récentes dans les Alpes françaises, Journal of Alpine Research
- 659 Revue de géographie alpine, 103–2, https://doi.org/10.4000/rga.2806, 2015.
- 660 Bolch, T., and Marchenko, S.: Significance of glaciers, rockglaciers and ice-rich permafrost in the Northern Tien Shan as water
- towers under climate change conditions, IHP/HWRP-Berichte, 8, Article 8, https://doi.org/10.5167/uzh-137250, 2009.
- 662 Brahney, J., Clague, J. J., Edwards, T. W. D., and Menounos, B.: Late Holocene paleohydrology of Kluane Lake, Yukon
- 663 Territory, Canada, Journal of Paleolimnology, 44(3), 873–885, https://doi.org/10.1007/s10933-010-9459-8, 2010.
- 664 Briggs, M. A., Hare, D. K., Boutt, D. F., Davenport, G., and Lane, J. W.: Thermal infrared video details multiscale groundwater
- discharge to surface water through macropores and peat pipes, Hydrological Processes, 30(14), 2510-2511,
- 666 https://doi.org/10.1002/hyp.10722, 2016.
- 667 Brighenti, S., Engel, M., Dinale, R., Tirler, W., Voto, G., and Comiti, F.: Isotopic and chemical signatures of high mountain
- 668 rivers in catchments with contrasting glacier and rock glacier cover, Journal of Hydrology, 623.
- https://doi.org/10.1016/j.jhydrol.2023.129779, 2023.
- 670 Brighenti, S., Tolotti, M., Bruno, M. C., Engel, M., Wharton, G., Cerasino, L., Mair, V., and Bertoldi, W.: After the peak
- water: The increasing influence of rock glaciers on alpine river systems, Hydrological Processes, 33(21), 2804–2823,
- 672 https://doi.org/10.1002/hyp.13533, 2019.
- 673 Brunner, P., Therrien, R., Renard, P., Simmons, C. T., and Franssen, H.-J. H.: Advances in understanding river-groundwater
- 674 interactions, Reviews of Geophysics, 55(3), 818–854, https://doi.org/10.1002/2017RG000556, 2017.
- 675 Carrivick, J. L., and Heckmann, T.: Short-term geomorphological evolution of proglacial systems, Geomorphology, 287, 3–
- 28, https://doi.org/10.1016/j.geomorph.2017.01.037, 2017.
- 677 Carturan, L., Zuecco, G., Andreotti, A., Boaga, J., Morino, C., Pavoni, M., Seppi, R., Tolotti, M., Zanoner, T., and Zumiani,
- 678 M.: Spring-water temperature suggests widespread occurrence of Alpine permafrost in pseudo-relict rock glaciers, EGUsphere,
- 679 1–35, https://doi.org/10.5194/egusphere-2023-2689, 2024.
- 680 Cartwright, I., and Hofmann, H.: Using radon to understand parafluvial flows and the changing locations of groundwater
- 681 inflows in the Avon River, southeast Australia, Hydrology and Earth System Sciences, 20(9), 3581–3600,
- 682 <u>https://doi.org/10.5194/hess-20-3581-2016, 2016.</u>
- 683 Casas-Mulet, R., Pander, J., Ryu, D., Stewardson, M. J., and Geist, J.: Unmanned Aerial Vehicle (UAV)-Based Thermal Infra-
- 684 Red (TIR) and Optical Imagery Reveals Multi-Spatial Scale Controls of Cold-Water Areas Over a Groundwater-Dominated
- Riverscape, Frontiers in Environmental Science, 8, https://doi.org/10.3389/fenvs.2020.00064, 2020.
- 686 Chakravarti, P., Jain, V., and Mishra, V.: The distribution and hydrological significance of intact rock glaciers in the north-
- 687 west Himalaya, Geografiska Annaler, Series A: Physical Geography, 104(3), 226-244,
- 688 <u>https://doi.org/10.1080/04353676.2022.2120262</u>, 2022.

- 689 Charonnat, B. and Baraer, M.: Supplemental Material: Drone-Based Thermal Infrared Imagery for Detection of Cold
- 690 Groundwater Exfiltration in Shár Shaw Tagà, Yukon, Canada, Borealis, V1, https://doi.org/10.5683/SP3/O57OMY, 2025.
- Chesnokova, A., Baraer, M., and Bouchard, É.: Proglacial icings as records of winter hydrological processes, The Cryosphere,
- 692 14(11), 4145–4164, https://doi.org/10.5194/tc-14-4145-2020, 2020.
- 693 Clow, D. W., Striegl, R. G., and Dornblaser, M. M.: Spatiotemporal Dynamics of CO2 Gas Exchange From Headwater
- Mountain Streams, Journal of Geophysical Research: Biogeosciences, 126(9), https://doi.org/10.1029/2021JG006509, 2021.
- 695 Colombo, N., Ferronato, C., Vittori Antisari, L., Marziali, L., Salerno, F., Fratianni, S., D'Amico, M. E., Ribolini, A., Godone,
- D., Sartini, S., Paro, L., Morra di Cella, U., and Freppaz, M.: A rock-glacier pond system (NW Italian Alps): Soil and
- 697 sediment properties, geochemistry, and trace-metal bioavailability, Catena, 194, https://doi.org/10.1016/j.catena.2020.104700,
- 698 2020.
- 699 Colombo, N., Gruber, S., Martin, M., Malandrino, M., Magnani, A., Godone, D., Freppaz, M., Fratianni, S., and Salerno, F.:
- Rainfall as primary driver of discharge and solute export from rock glaciers: The Col d'Olen Rock Glacier in the NW Italian
- 701 Alps, Science of the Total Environment, 639, 316–330, https://doi.org/10.1016/j.scitotenv.2018.05.098, 2018.
- 702 Colombo, N., Salerno, F., Martin, M., Malandrino, M., Giardino, M., Serra, E., Godone, D., Said-Pullicino, D., Fratianni, S.,
- 703 Paro, L., Tartari, G., and Freppaz, M.: Influence of permafrost, rock and ice glaciers on chemistry of high-elevation ponds
- 704 (NW Italian Alps), Science of the Total Environment, 685, 886–901, https://doi.org/10.1016/j.scitotenv.2019.06.233, 2019.
- 705 Colucci, R. R., Forte, E., Žebre, M., Maset, E., Zanettini, C., and Guglielmin, M. Is that a relict rock glacier? Geomorphology,
- 706 330, 177–189, https://doi.org/10.1016/j.geomorph.2019.02.002, 2019.
- 707 Croce, F., and Milana, J.: Internal structure and behavior of a Rock Glacier in the arid Andes of Argentina, Permafrost and
- 708 Periglacial Processes, 13, 289–299, https://doi.org/10.1002/ppp.431, 2002.
- 709 Del Siro, C., Scapozza, C., Perga, M.-E., & Lambiel, C.: Investigating the origin of solutes in rock glacier springs in the Swiss
- Alps: A conceptual model, Frontiers in Earth Science, 11, https://doi.org/10.3389/feart.2023.1056305, 2023.
- 711 Delaloye, R., Lambiel, C., and Gärtner-Roer, I.: Overview of rock glacier kinematics research in the Swiss Alps: Seasonal
- 712 rhythm, interannual variations and trends over several decades, Geographica Helvetica, 65(2), 135-145,
- 713 https://doi.org/10.5194/gh-65-135-2010, 2010.
- 714 Dodds, C.J., and Campbell, R.B.: Overview, legend and mineral deposit tabulations for: GSC Open File 2188 to Open File
- 715 2191, Geological Survey of Canada, Energy Mines and Resources Canada, 85 p. + 5 maps, 1992.
- 716 Dugdale S. J.: A practitioner's guide to thermal infrared remote sensing of rivers and streams: recent advances, precautions
- 717 and considerations, WIREs Water, vol. 3, no. 2, pp. 251–268, https://doi.org/10.1002/wat2.1135, 2016.
- 718 Engel, M., Penna, D., Bertoldi, G., Vignoli, G., Tirler, W., and Comiti, F.: Controls on spatial and temporal variability in
- 719 streamflow and hydrochemistry in a glacierized catchment, Hydrology and Earth System Sciences, 23(4), 2041–2063,
- 720 <u>https://doi.org/10.5194/hess-23-2041-2019</u>, 2019.

- Ensom, T., Makarieva, O., Morse, P., Kane, D., Alekseev, V., and Marsh, P.: The distribution and dynamics of aufeis in
- permafrost regions, Permafrost and Periglacial Processes, 31(3), 383–395, https://doi.org/10.1002/ppp.2051, 2020.
- 723 Evin, M., Fabre, D., and Johnson, P. G.: Electrical Resistivity Measurements on the Rock Glaciers of Grizzly Creek, St Elias
- Mountains, Yukon, Permafrost and Periglacial Processes, 8, 11, 1997.
- 725 Falatkova, K., Šobr, M., Slavík, M., Bruthans, J., and Janský, B.: Hydrological characterization and connectivity of proglacial
- lakes to a stream, Adygine ice-debris complex, northern Tien Shan, Hydrological Sciences Journal, 65(4), 610-623,
- 727 https://doi.org/10.1080/02626667.2020.1711913, 2020.
- 728 Frauenfelder, R., Allgöwer, B., Haeberli, W., and Hoelzle, M.: Permafrost investigations with GIS a case study in the
- 729 Fletschhorn area, Wallis, Swiss Alps, In Permafrost, Proceedings of the Seventh International Conference, 23–27 June 1998,
- 730 Yellowknife, Canada, Lewkowicz AG, Allard M (eds) eds, Collection Nordicana 57, Centre d'études Nordiques, Université
- 731 Laval: Québec; 291–295, 1998.
- Gammons, C. H., Doolittle, M. F., Eastman, K. A., and Poulson, S. R.: Geochemistry of natural acid rock drainage in the Mt
- 733 Evans area, Anaconda-Pintler Range, Montana, USA, Geochemistry: Exploration, Environment, Analysis, 21(4),
- 734 https://doi.org/10.1144/geochem2021-068, 2021.
- 735 Gibson J.J., Holmes T., Stadnyk T.A., Birks S.J., Eby P., and Pietroniro A.: 18O and <sup>2</sup>H in streamflow across Canada, Journal
- 736 of Hydrology: Regional Studies, Volume 32, 100754, ISSN 2214-5818, https://doi.org/10.1016/j.ejrh.2020.100754, 2020.
- 737 Haeberli, W.: Untersuchungen zur Verbreitung von Permafrost zwischen Flüelapass und Piz Grialetsch (Graubünden),
- 738 Mitteilungen der VAW ETH Zürich 17: 1–221, 1975.
- Halla, C., Henrik Blöthe, J., Tapia Baldis, C., Trombotto Liaudat, D., Hilbich, C., Hauck, C., and Schrott, L.: Ice content and
- 740 interannual water storage changes of an active rock glacier in the dry Andes of Argentina, Cryosphere, 15(2), 1187–1213,
- 741 https://doi.org/10.5194/tc-15-1187-2021, 2021.
- 742 Harrington, J. S., Mozil, A., Hayashi, M., and Bentley, L. R.: Groundwater flow and storage processes in an inactive rock
- 743 glacier, Hydrological Processes, 32(20), 3070–3088, https://doi.org/10.1002/hyp.13248, 2018.
- Harrison, S., Jones, D., Anderson, K., Shannon, S., and Betts, R. A.: Is ice in the Himalayas more resilient to climate change
- 745 than we thought? Geografiska Annaler, Series A: Physical Geography, 103(1), 1-7,
- 746 https://doi.org/10.1080/04353676.2021.1888202, 2021.
- 747 Hayashi, M.: Alpine Hydrogeology: The Critical Role of Groundwater in Sourcing the Headwaters of the World. Groundwater,
- 748 58(4), 498–510, https://doi.org/10.1111/gwat.12965, 2020.
- 749 Hem, J. D.: Study and Interpretation of the Chemical Characteristics of Natural Water, 3rd Edition, US Geological Survey
- Water-Supply Paper 2254, University of Virginia, Charlottesville, 263 p., <a href="https://doi.org/10.3133/wsp2254">https://doi.org/10.3133/wsp2254</a>, 1985.
- 751 Hewitt, K.: Rock Glaciers and Related Phenomena. In K. Hewitt (Ed.), Glaciers of the Karakoram Himalaya: Glacial
- Environments, Processes, Hazards and Resources (pp. 267–289), Springer Netherlands, <a href="https://doi.org/10.1007/978-94-007-289">https://doi.org/10.1007/978-94-007-289</a>), Springer Netherlands, <a href="https://doi.org/10.1007/978-289">https://doi.org/10.1007/978-299</a>), Springer Netherlands, <a href="https://doi.org/10.1007/978-299">https://doi.org/10.1007/978-299</a>), Springer Netherlands, <a href="https://doi.org/10.1007/978-299</a>), Springer Netherlands, <a hr
- 753 6311-1 11, 2014.

- Hock, R., Rasul, G., Adler, C., Cáceres, B., Gruber, S., Hirabayashi, Y., Jackson, M., Kääb, A., Kang, S., Kutuzov, S., Milner,
- 755 Al., Molau, U., Morin, S., Orlove, B., and Steltzer, H.: High Mountain Areas. In: IPCC Special Report on the Ocean and
- 756 Cryosphere in a Changing Climate [Pörtner, H.-O., Roberts, D.C., Masson-Delmotte, V., Zhai, P., Tignor, M., Poloczanska,
- 757 E., Mintenbeck, K., Alegría, A., Nicolai, M., Okem, A., Petzold, J., Rama, B. and Weyer N.M. (eds.)]: Cambridge University
- 758 Press, Cambridge, UK and New York, NY, USA, pp. 131-202, https://doi.org/10.1017/9781009157964.004, 2019.
- 759 Hu, X., and Pollard, W.H.: The hydrologic analysis and modelling of river icing growth, North Fork Pass, Yukon Territory,
- 760 Canada, Permafrost and Periglacial Processes, 8: 279–294, https://doi.org/10.1002/(SICI)1099-1530(199709)8:3<279::AID-
- 761 PPP260>3.0.CO:2-7, 1997.
- Huss, M., Bookhagen, B., Huggel, C., Jacobsen, D., Bradley, R. S., Clague, J. J., Vuille, M., Buytaert, W., Cayan, D. r.,
- 763 Greenwood, G., Mark, B. g., Milner, A. M., Weingartner, R., and Winder, M.: Toward mountains without permanent snow
- 764 and ice, Earth's Future, 5(5), 418–435, https://doi.org/10.1002/2016EF000514, 2017.
- 765 Iwasaki, K., Fukushima, K., Nagasaka, Y., Ishiyama, N., Sakai, M., and Nagasaka, A.: Real-Time Monitoring and
- 766 Postprocessing of Thermal Infrared Video Images for Sampling and Mapping Groundwater Discharge, Water Resources
- 767 Research, 59(4), e2022WR033630, https://doi.org/10.1029/2022WR033630, 2023.
- 768 Iwasaki, K., Nagasaka Y., Ishiyama N., and Nagasaka A.: Thermal imaging survey for characterizing bedrock groundwater
- 769 discharge: comparison between sedimentary and volcanic catchments, Hydrological Research Letters 18(3): 79-86,
- 770 http://dx.doi.org/10.3178/hrl.18.79, 2024.
- Johnson, P. G.: Holocene Paleohydrology of the St. Elias Mountains, British Columbia and Yukon, Géographie Physique et
- 772 Quaternaire, 40(1), 47–53, https://doi.org/10.7202/032622ar, 1986.
- Johnson, P. G.: Mass Movement of Ablation Complexes and Their Relationship to Rock Glaciers, Geografiska Annaler, Series
- 774 A, Physical Geography, 56(1/2), 93–101, https://doi.org/10.2307/520430, 1974.
- Johnson, P. G.: Rock glacier types and their drainage systems, Grizzly Creek, Yukon Territory, Canadian Journal of Earth
- 776 Sciences, 15(9), 1496–1507, https://doi.org/10.1139/e78-155, 1978.
- Johnson, P. G.: Glacier-Rock Glacier Transition in the Southwest Yukon Territory, Canada, Arctic and Alpine Research, 12(2),
- 778 195, https://doi.org/10.2307/1550516, 1980.
- Johnson, P. G.: Rock Glaciers, A Case for a Change in Nomenclature, Geografiska Annaler, Series A, Physical Geography,
- 780 65(1/2), 27–34, https://doi.org/10.2307/520718, 1983.
- 781 Johnson, P. G.: Stagnant Glacier Ice, St. Elias Mountains, Yukon, Geografiska Annaler, Series A, Physical Geography, 74(1),
- 782 13–19, https://doi.org/10.2307/521466, 1992.
- Jones, D. B., Harrison, S., Anderson, K., and Betts, R. A.: Mountain rock glaciers contain globally significant water stores,
- 784 Scientific Reports, 8(1), Article 1, https://doi.org/10.1038/s41598-018-21244-w, 2018.
- Jones, D. B., Harrison, S., Anderson, K., Shannon, S., and Betts, R. A.: Rock glaciers represent hidden water stores in the
- 786 Himalaya, Science of The Total Environment, 793, 145368, https://doi.org/10.1016/j.scitotenv.2021.145368, 2021.

- Jones, D. B., Harrison, S., Anderson, K., and Whalley, W. B.: Rock glaciers and mountain hydrology: A review, Earth-Science
- 788 Reviews, 193, 66–90, https://doi.org/10.1016/j.earscirev.2019.04.001, 2019.
- 789 Kalbus, E., Reinstorf, F., and Schirmer, M.: Measuring methods for groundwater and surface water interactions: review,
- 790 Hydrology and Earth System Sciences, 10(6), 873–887, https://doi.org/10.5194/hess-10-873-2006, 2006.
- Käser, D., and Hunkeler, D.: Contribution of alluvial groundwater to the outflow of mountainous catchments, Water Resources
- 792 Research, 52(2), 680–697, https://doi.org/10.1002/2014WR016730, 2016.
- 793 Krainer, K., and Mostler, W.: Hydrology of Active Rock Glaciers: Examples from the Austrian Alps, Arctic, Antarctic, and
- 794 Alpine Research, 34(2), 142–149, https://doi.org/10.1080/15230430.2002.12003478, 2002.
- 795 Krainer, K., Mostler, W., and Spötl, C.: Discharge from active rock glaciers, Austrian Alps: A stable isotope approach, Austrian
- 796 Journal of Earth Sciences, 100, 102–112, 2007.
- 797 Kummert, M., Bodin, X., Braillard, L., and Delaloye, R.: Pluri-decadal evolution of rock glaciers surface velocity and its
- impact on sediment export rates towards high alpine torrents, Earth Surface Processes and Landforms, 46(15), 3213–3227,
- 799 https://doi.org/10.1002/esp.5231, 2021.
- 800 Liu, W., Fortier, R., Molson, J., and Lemieux, J.: A conceptual model for talk dynamics and icing formation in a river
- 801 floodplain in the continuous permafrost zone at Salluit, Nunavik (Quebec), Canada, Permafrost and Periglacial Processes,
- 32(3), 468–483, https://doi.org/10.1002/ppp.2111, 2021.
- 803 Lloyd, S.: Least squares quantization in PCM, IEEE Transactions on Information Theory, 28(2), 129–137, IEEE Transactions
- on Information Theory, https://doi.org/10.1109/TIT.1982.1056489, 1982.
- 805 MacQueen, J.: Some methods for classification and analysis of multivariate observations, In Proceedings of the fifth Berkeley
- symposium on mathematical statistics and probability (Vol. 1, No. 14, pp. 281-297), 1967.
- 807 Mallinson, L., Swift, D. A., and Sole, A.: Proglacial icings as indicators of glacier thermal regime: Ice thickness changes and
- 808 icing occurrence in Svalbard, Geografiska Annaler, Series A: Physical Geography, 101(4), 334-349,
- 809 https://doi.org/10.1080/04353676.2019.1670952, 2019.
- 810 Marcer, M., Cicoira, A., Cusicanqui, D., Bodin, X., Echelard, T., Obregon, R., and Schoeneich, P.: Rock glaciers throughout
- the French Alps accelerated and destabilised since 1990 as air temperatures increased, Communications Earth & Environment,
- 812 2(1), 1–11, https://doi.org/10.1038/s43247-021-00150-6, 2021.
- 813 Marren, P. M., and Toomath, S. C.: Channel pattern of proglacial rivers: Topographic forcing due to glacier retreat, Earth
- 814 Surface Processes and Landforms, 39(7), 943–951, https://doi.org/10.1002/esp.3545, 2014.
- Müller, T., Lane, S. N., and Schaefli, B.: Towards a hydrogeomorphological understanding of proglacial catchments: An
- assessment of groundwater storage and release in an Alpine catchment, Hydrology and Earth System Sciences, 26(23), 6029–
- 817 6054, https://doi.org/10.5194/hess-26-6029-2022, 2022.

- Müller, T., Roncoroni, M., Mancini, D., Lane, S. N., and Schaefli, B.: Current and future roles of meltwater-groundwater
- 819 dynamics in a proglacial Alpine outwash plain, Hydrology and Earth System Sciences, 28(4), 735-759,
- 820 https://doi.org/10.5194/hess-28-735-2024, 2024.
- 821 Navarro, G., Valois, R., MacDonell, S., de Pasquale, G., and Díaz, J. P.: Internal structure and water routing of an ice-debris
- 822 landform assemblage using multiple geophysical methods in the semiarid Andes, Frontiers in Earth Science, 11,
- 823 https://doi.org/10.3389/feart.2023.1102620, 2023.
- PERMOS Report 2019-16-19 | PERMOS Swiss Permafrost Monitorinig Network, Retrieved 17 September 2024, from
- 825 https://www.permos.ch/doi/permos-rep-2019-16-19, 2019.
- Porter, C., Howat, I., Noh, M.-J., Husby, E., Khuvis, S., Danish, E., Tomko, K., Gardiner, J., Negrete, A., Yadav, B., Klassen,
- 827 J., Kelleher, C., Cloutier, M., Bakker, J., Enos, J., Arnold, G., Bauer, G., and Morin, P.: ArcticDEM Mosaics, Version 4.1
- [Dataset], Harvard Dataverse, https://doi.org/10.7910/DVN/3VDC4W, 2023.
- 829 Rautio, A., Kivimäki, A.-L., Korkka-Niemi, K., Nygård, M., Salonen, V.-P., Lahti, K., and Vahtera, H.: Vulnerability of
- groundwater resources to interaction with river water in a boreal catchment, Hydrology and Earth System Sciences, 19(7),
- 831 3015–3032, https://doi.org/10.5194/hess-19-3015-2015, 2015.
- 832 Reato, A., Borzi, G., Martínez, O. A., and Carol, E.: Role of rock glaciers and other high-altitude depositional units in the
- hydrology of the mountain watersheds of the Northern Patagonian Andes, Science of The Total Environment, 824, 153968,
- https://doi.org/10.1016/j.scitotenv.2022.153968, 2022.
- 835 Robinson, C. T., Jolidon, C., Consoli, G., Bloem, S., and Ebi, C.: Temporal dynamics in the physico-chemistry of a high-
- alpine stream network in the Swiss National Park, Eco.Mont, 14(2), 11–23, https://doi.org/10.1553/eco.mont-14-2s11, 2022.
- 837 Scapozza, C.: Contributo dei metodi termici alla prospezione del permafrost montano: esempi dal massiccio della Cima di
- 838 Gana Bianca (Val Blenio, Svizzera), Bollettino della Società Ticinese di Scienze Naturali 97:55–66, 2009.
- 839 Scapozza, C.: Investigation on protalus ramparts in the Swiss Alps, Geographica Helvetica, 70(2), 135-139,
- 840 https://doi.org/10.5194/gh-70-135-2015, 2015.
- 841 Schreder, S., Sommaruga, R., Psenner, R., Chimani, B., Ganekind, M., and Koinig, K. A.: Changes in air temperature, but not
- 842 in precipitation, determine long-term trends in water chemistry of high mountain lakes of the Alps with and without rock
- glacier influence, Science of the Total Environment, 905, <a href="https://doi.org/10.1016/j.scitotenv.2023.167750">https://doi.org/10.1016/j.scitotenv.2023.167750</a>, 2023.
- 844 Scotti, R., Crosta, G. B., and Villa, A.: Destabilisation of Creeping Permafrost: The Plator Rock Glacier Case Study (Central
- Italian Alps), Permafrost and Periglacial Processes, 28(1), 224–236, https://doi.org/10.1002/ppp.1917, 2017.
- 846 Sorg, A., Kääb, A., Roesch, A., Bigler, C., and Stoffel, M.: Contrasting responses of Central Asian rock glaciers to global
- warming, Scientific Reports, 5, <a href="https://doi.org/10.1038/srep08228">https://doi.org/10.1038/srep08228</a>, 2015.
- Terry, N., Grunewald, E., Briggs, M., Gooseff, M., Huryn, A. D., Kass, M. A., Tape, K. D., Hendrickson, P., and Lane, J. W.,
- Jr.: Seasonal Subsurface Thaw Dynamics of an Aufeis Feature Inferred From Geophysical Methods, Journal of Geophysical
- 850 Research: Earth Surface, 125(3), https://doi.org/10.1029/2019JF005345, 2020.

- 851 Tjoelker, A., Baraer, M., Valence, E., Charonnat, B., Masse-Dufresne, J., Mark, B., and McKenzie, J.: Drone-Based Ground-
- Penetrating Radar with Manual Transects for Improved Field Surveys of Buried Ice, Remote Sensing, 16, 2461,
- 853 https://doi.org/10.3390/rs16132461, 2024.
- 854 Toran, L.: Groundwater-Surface Water Interaction, In Encyclopedia of Water (pp. 1-12), John Wiley & Sons, Ltd,
- https://doi.org/10.1002/9781119300762.wsts0027, 2019.
- 856 Torgersen C. E., Faux R. N., McIntosh B. A., Poage N. J., and Norton D. J.: Airborne thermal remote sensing for water
- 857 temperature assessment in rivers and streams, Remote Sensing of Environment, vol. 76, no. 3, pp. 386–398,
- https://doi.org/10.1016/S0034-4257(01)00186-9, 2001.
- 859 Tronstad, L. M., Hotaling, S., Giersch, J. J., Wilmot, O. J., and Finn, D. S.: Headwaters Fed by Subterranean Ice: Potential
- 860 Climate Refugia for Mountain Stream Communities? Western North American Naturalist, 80(3), 395-407,
- 861 https://doi.org/10.3398/064.080.0311, 2020.
- van Tiel, M., Aubry-Wake, C., Somers, L., Andermann, C., Avanzi, F., Baraer, M., Chiogna, G., Daigre, C., Das, S., Drenkhan,
- 863 F., Farinotti, D., Fyffe, C. L., de Graaf, I., Hanus, S., Immerzeel, W., Koch, F., McKenzie, J. M., Müller, T., Popp, A. L., ...
- Yapiyev, V.: Cryosphere–groundwater connectivity is a missing link in the mountain water cycle, Nature Water, 2(7), 624–
- 865 637, https://doi.org/10.1038/s44221-024-00277-8, 2024.
- 866 Vélez-Nicolás, M., García-López, S., Barbero, L., Ruiz-Ortiz, V., and Sánchez-Bellón, Á.: Applications of Unmanned Aerial
- 867 Systems (UASs) in Hydrology: A Review, Remote Sensing, 13(7), Article 7, https://doi.org/10.3390/rs13071359, 2021.
- Wagner, T., Brodacz, A., Krainer, K., and Winkler, G.: Active rock glaciers as shallow groundwater reservoirs, Austrian Alps,
- 869 Grundwasser, 25(3), 215–230, https://doi.org/10.1007/s00767-020-00455-x, 2020.
- Wagner, T., Kainz, S., Krainer, K., and Winkler, G.: Storage-discharge characteristics of an active rock glacier catchment in
- the Innere Ölgrube, Austrian Alps, Hydrological Processes, 35(5), https://doi.org/10.1002/hyp.14210, 2021.
- Wagner, T., Pauritsch, M., and Winkler, G.: Impact of relict rock glaciers on spring and stream flow of alpine watersheds:
- 873 Examples of the Niedere Tauern Range, Eastern Alps (Austria), Austrian Journal of Earth Sciences, 109(1),
- 874 https://doi.org/10.17738/ajes.2016.0006, 2016.
- Wahl, H. E., Fraser, D. B., Harvey, R. C., and Maxwell, J. B.: Climate of Yukon, Atmospheric Environment Service,
- 876 Environment Canada, 1987.
- Wainstein, P., Moorman, B., and Whitehead, K.: Glacial conditions that contribute to the regeneration of Fountain Glacier
- proglacial icing, Bylot Island, Canada, Hydrological Processes, 28(5), 2749–2760, https://doi.org/10.1002/hyp.9787, 2014.
- Wanner, C., Moradi, H., Ingold, P., Cardenas Bocanegra, M. A., Mercurio, R., and Furrer, G.: Rock glaciers in the Central
- 880 Eastern Alps How permafrost degradation can cause acid rock drainage, mobilization of toxic elements and formation of
- basaluminite, Global and Planetary Change, 227, https://doi.org/10.1016/j.gloplacha.2023.104180, 2023.
- Webb, B. W., Hannah, D. M., Moore, R. D., Brown, L. E., and Nobilis, F.: Recent advances in stream and river temperature
- 883 research, Hydrological Processes, 22(7), 902–918, https://doi.org/10.1002/hyp.6994, 2008.

- Winkler, G., Wagner, T., Pauritsch, M., and Kellerer-Pirklbauer, A.: What will occur after permafrost? Relevance of relict
- rock glaciers for the discharge behaviour of alpine catchments, Joannea Geologie und Palaontologie, 12, 63–72, 2016.
- Zappa C. J., Jessup A. T., and Yeh H.: Skin layer recovery of free-surface wakes: Relationship to surface renewal and
- dependence on heat flux and background turbulence, Journal of Geophysical Research: Oceans, vol. 103, no. C10, pp. 21711–
- 888 21722, 1998, https://doi.org/10.1029/98JC01942, 1998.
- 889 Zarroca, M., Roqué, C., Linares, R., Salminci, J. G., and Gutiérrez, F.: Natural acid rock drainage in alpine catchments: A side
- effect of climate warming, Science of The Total Environment, 778, 146070, https://doi.org/10.1016/j.scitotenv.2021.146070,
- 891 2021.
- 892 Zierl, B., and Bugmann, H.: Global change impacts on hydrological processes in Alpine catchments, Water Resources
- 893 Research, 41(2), <a href="https://doi.org/10.1029/2004WR003447">https://doi.org/10.1029/2004WR003447</a>, 2005.